communications earth & environment

Article

https://doi.org/10.1038/s43247-024-01386-8

Influence of large-scale circulation and local feedbacks on extreme summer heat in Argentina in 2022/23

Check for updates

Soledad Collazo [1,2,3] ✉, Solange Suli [1,2,3], Pablo G. Zaninelli[3], Ricardo García-Herrera [1,3], David Barriopedro [3] & José M. Garrido-Perez [1]

The summer of 2022/23 in Argentina set a record with ten heatwaves. Here, we compare the synoptic and thermodynamic conditions of the four heatwaves with the largest spatial extent using ERA5 reanalysis data. All heatwaves were associated with mid-level anticyclonic anomalies but with different characteristics: three were quasi-stationary high-pressure systems, while one was transient. We also find that enhanced surface fluxes strongly influenced the daily temperature evolution. Furthermore, we perform an attribution exercise using the analogue technique to measure the contributions of atmospheric circulation, soil moisture, and climate change. For quasi-stationary events, the main contribution came from the circulation (up to 2 °C relative to random flow in the present climate). Conversely, the transient heatwave showed a stronger association with extreme soil moisture deficits, with an estimated increase of ~+1 °C relative to wetter conditions. Climate change has also increased the intensity of heatwaves by +0.5 to +1.2 °C relative to previous decades.

The summer of 2022/23 in Argentina was unusually warm[1], being the hottest in the last 60 years. During the extended warm season from November 2022 to March 2023, Argentina experienced an exceptional number of ten heatwaves, differing in intensity, geographical extent, and duration[2,3]. The November-January 2022/23 quarter proved to be the warmest (+1.7 °C) in 60 years of records, with several locations across the country experiencing record-breaking daily maximum temperatures (TX). For instance, Bariloche in Patagonia recorded its highest November TX (32.5 °C) since 1961[4]. In December 2022, TX reached 44 °C at several locations in the north (e.g., Tucumán)[5]. Although no record-breaking TX was evidenced in January 2023, various weather stations in the south experienced annual records in minimum temperatures (e.g., Viedma, 26.3 °C)[6]. In February, Ezeiza Airport set both maximum and minimum temperature records (39.6 °C and 27.8 °C, respectively)[7]. Similarly, in March 2023, new records were set over central-eastern Argentina. In particular, Buenos Aires recorded a historic TX (38.9 °C), a value that had never been observed in the city in the last 117 years of recorded data[3] (station locations are shown in Supplementary Fig. 1).

Previous studies have analysed the atmospheric circulation associated with mid-latitude heatwaves (e.g., Barriopedro et al.[8]; Geirinhas et al.[9] and references therein). These extreme events are typically characterised by anomalous large-scale circulation, such as atmospheric blocking (e.g., Sousa et al.[10]), subtropical ridges (e.g., Wang et al.[11]), and Rossby wave packets (e.g., Fragkoulidis et al.[12]). Specifically, South American heatwaves exhibit regional differences[13]. Subtropical South American heatwaves are triggered by persistent co-located anticyclonic patterns, which can be attributed to shifts or intensification of subtropical semi-permanent high-pressure systems[9,14]. Conversely, southern South American heatwaves are driven by extratropical systems that block the westerly flow. All of these processes can lead to warm temperature advection, and adiabatic warming by subsidence and/or diabatic heating, promoting a favourable environment for the occurrence of heatwaves[13].

Remote drivers, such as the South Atlantic Convergence Zone (SACZ) or the South American Low-Level Jet (SALLJ), have also been suggested to play an important role in the development of South American summer heatwaves (e.g., Cerne and Vera[15]). Regional studies have demonstrated that an active SACZ promotes subsidence and anticyclonic circulation over south-eastern South America, increasing temperatures in the region[16]. In addition, Cerne et al.[17] provide evidence that the intensification of the SALLJ results in warm and moist advection from the Amazon basin towards south-eastern South America, which plays a crucial role in the development of

[1]Departamento de Física de la Tierra y Astrofísica, Facultad de Ciencias Físicas, Universidad Complutense de Madrid (UCM), Plaza de las Ciencias 1, Madrid, Spain. [2]Departamento de Ciencias de la Atmósfera y los Océanos, Facultad de Ciencias Exactas y Naturales, Universidad de Buenos Aires (FCEN, UBA), Buenos Aires, Argentina. [3]Instituto de Geociencias (IGEO), Consejo Superior de Investigaciones Científicas–Universidad Complutense de Madrid (CSIC–UCM), Madrid, Spain. ✉e-mail: scollazo@ucm.es

heatwaves in central Argentina. Furthermore, Liebmann et al.[18] report an anomalous dipole pattern between SACZ activity and the SALLJ strength. They observe that enhanced (suppressed) convection over the SACZ corresponds to a weakening (strengthening) of the SALLJ.

Interannual variability also contributes to the development of heatwaves in South America. The El Niño–Southern Oscillation (ENSO) is one of the most important drivers of year-to-year variability in weather patterns worldwide[19]. In north-eastern Argentina, the most pronounced impact of ENSO tends to occur from September to March, where above-average (below-average) precipitation is observed during El Niño (La Niña) phases[20,21]. In 2022, Argentina experienced its third consecutive year of devastating drought due to persistent triple-dip La Niña conditions[22] —a rare phenomenon that had only occurred twice in the preceding 60 years. This outstanding 2020–2023 La Niña event has been identified as the primary driver behind precipitation deficits, severe soil desiccation, and extreme drought in central-eastern South America[23].

Prolonged drought can have a major effect on soil moisture[24] and thus on the balance of turbulent heat fluxes[25,26]. Dry soil conditions increase the influence of soil moisture content on evapotranspiration in regions with a transitional regime (an intermediate state between arid and humid conditions)[25], leading to soil moisture-atmosphere coupling[25,27–30]. Several previous works have indicated south-eastern South America as one of the main hot spots of soil moisture-atmosphere coupling in the continent[26–28]. Moreover, substantial effort has been devoted to investigating the relationship between soil conditions and temperature patterns, including their variability[29,30]. Coronato et al.[31] show that the impact of anomalous dry/wet soil conditions on the intensity and duration of hot days is amplified when there is soil-atmosphere coupling. However, all these studies have examined the soil moisture-atmosphere feedback from a climatological perspective or explored its potential impacts under climate change scenarios[30,32,33]. Recent studies focusing on South America have also linked the strong soil-atmosphere coupling to the occurrence of specific heatwave events. For example, a strong soil moisture-temperature coupling led to record-breaking temperatures in south-eastern Brazil in 2013/14, exceeding the previous record by almost 5 °C, and played a crucial role in the initiation of an exceptional mega-heatwave that persisted for approximately 20 days[34]. Furthermore, Libonati et al.[35] emphasise the importance of the compound drought-heatwave event as a trigger for the extensive fires in the Brazilian Pantanal in 2020.

The objective of this study is to characterise the four most extensive heatwaves recorded during the hottest summer of 2022/23 in Argentina. To achieve this, three complementary analyses are conducted: synoptic analysis based on circulation composites, thermodynamic analysis based on the daily evolution of temperature tendency, and attribution analysis based on the application of the analogue technique. In particular, the latter analysis considers the role of atmospheric circulation, extreme drought and climate change in the TX anomalies recorded during the heatwaves.

During the warm season of 2022/23, heatwave events were characterised by the presence of both quasi-stationary and transient anticyclonic anomalies in the mid-level atmosphere. These anomalies led to clear skies, subsidence, and warming conditions. Additionally, diabatic heating was the primary driver of daily temperature variations during the life cycle of these events. The attribution analysis reveals that atmospheric circulation plays the most relevant role in driving all heatwaves except the transient one, increasing TX anomalies by up to ~2 °C relative to a random flow under current climate conditions. The amplification of the heatwaves was also strongly influenced by the extremely dry soil conditions resulting from successive La Niña years and the soil-atmosphere coupling, which proved to be the main driver of the transient event. Finally, we demonstrate that global warming has also contributed to an increase in the intensity of these heatwaves, ranging from 0.5 to 1.2 °C relative to the 1951–1980 period.

Results and discussion

To provide context for the extended summer (NDJFM) of 2022/23, we analyse the standardised anomalies of TX in southern South America (80-45°W 60-20°S) using ERA5 data. Figure 1a shows widespread warm anomalies over most of Argentina, with the central and northern regions experiencing the highest anomalies, deviating by over four standard deviations from the seasonal mean. The remarkable extension and intense nature of these deviations led to the entire southern South America experiencing an average anomaly of 1.56 °C above the 1981–2010 baseline, marking the highest values recorded since 1950 (Fig. 1b). As shown in Fig. 1b, anomalously warm NDJFM seasons have become more frequent over the last century, which could be an indication of climate change. Furthermore, by examining the ranking of anomalies for each grid point (Fig. 1c), we observe that the extended summer of 2022/23 was the warmest on record (1951–2023) in a large part of Argentina.

Regarding TX extremes, over 40% of warm season days in the central region of the country were classified as a heatwave day (Fig. 1d). Furthermore, over 60% of the season's days experienced strong heat stress conditions according to the Universal Thermal Climate Index (Supplementary Fig. 2a), which is 25% higher than expected based on climatology (Supplementary Fig. 2b, c). Thus, the local population was exposed to a higher thermal stress than they are adapted to, with possible negative consequences for their health[36]. According to reports from the National Meteorological Service (SMN)[2], Argentina experienced ten remarkable heatwaves during the warm season, setting a new record for the country. This study examines the four heatwaves with the largest spatial extent, each covering more than 1.5 million km^2 (Table 1), according to the heatwave algorithm[37] (details in Section "Heat waves detection"). Moreover, the algorithm calculates additional metrics to characterise the events (Table 1). Each of the four heatwaves occurred in a different month and lasted from 7 to 17 days. In terms of mean intensity, they all had comparable values. The names of the events were selected based on the prevailing synoptic forcing, as discussed below.

Another crucial aspect of the season was that it occurred during the third consecutive year of La Niña conditions. The persistent La Niña event was already identified as the main driver of the severe drought in central-eastern South America[23,38], a condition that has worsened over time[39]. Figure 1e displays the standardised soil moisture anomalies during the 2022/23 warm season. Extensive soil moisture deficits were record-breaking in the northern half of the country, considering data since 1950/51 (Fig. 1f). This is consistent with the findings of Arias et al.[38], who reported that 2022 was the driest year in central Argentina since 1960. These record precipitation and soil moisture deficits meant that much of the region also experienced sensible heat fluxes (SHFs) above three standard deviations of the mean (Fig. 1g), which were also record-breaking in a large part of northern Argentina (Fig. 1h). Thus, regions affected by extreme temperatures coincide with areas where soils were exceptionally dry and produced high SHFs.

Pacific anticyclone heatwave (PAHW)

PAHW occurred from 02 December to 15 December and mainly affected central and northern Argentina (Fig. 2a). This event corresponds to the area identified by the SMN, characterized by an unusual incidence of extremely high TX, exceeding up to 40 °C on multiple days[5]. Regarding the associated atmospheric circulation, PAHW experienced significant positive geopotential height anomalies at 500hPa (Z500), centred around 70°W and extending over the South Pacific and central-northern Argentina (Fig. 2b). These anomalies led to atmospheric stability and reduced convection (Fig. 2c), promoting clear skies that are associated with radiative heating and strong SHFs (Supplementary Fig. 3a), and facilitating the heatwave occurrence. In contrast, cyclonic anomalies, such as those observed in southern Argentina, are typically not associated with heatwaves in this region.

Radiative heating and SHFs are processes included in the diabatic term of the thermodynamic equation (Eq. (3) in "Methods"). During PAHW, this term played a key role in driving temperature changes, favouring warming at the beginning and end of the event (Fig. 2d). It is worth noting that horizontal thermal advection contributed to the temperature increase between 05 and 09 December, while it contributed to cooling towards the end of the heatwave. During the period characterised by warm horizontal advection, different trajectories of air masses reached central Argentina

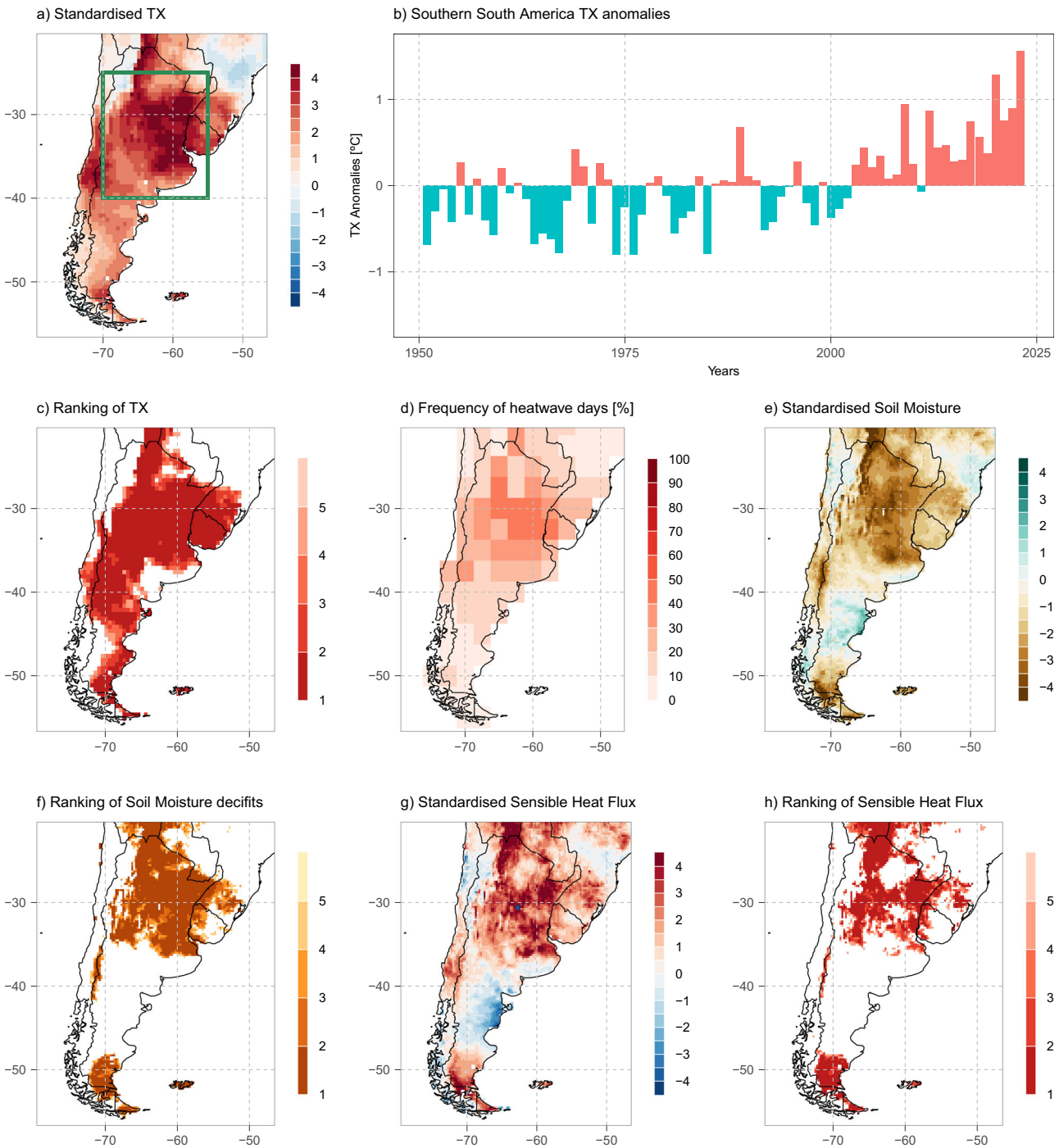

Fig. 1 | Warm season 2022/23 in Argentina. a Standardised maximum temperature (TX) anomalies [°C] in the warm season 2022/23 (NDJFM) with respect to the period 1981–2010. **b** Spatial average over land in southern South America (80-45°W, 60-20°S) of the mean seasonal TX anomalies. **c** Ranking of the TX of the warm season 2022/23 compared to all warm seasons since 1950/51. **d** Relative frequency of heat wave days during the warm season 2022/23. **e** Standardised water volume anomalies in soil layer 1 (0–7 cm, the surface is at 0 cm) in the warm season 2022/23. **f** Ranking of soil moisture deficits in the warm season 2022/23 compared to all warm seasons since 1950/51. **g** Standardised surface sensible heat flux anomalies in the warm season 2022/23. **h** Ranking of surface sensible heat flux in the warm season 2022/23 compared to all warm seasons since 1950/51. The rectangle in (**a**) indicates the area where the thermodynamic equation is averaged, and where soil moisture is considered in the analogue study. *Credit line: The maps were created by the first author using the ggplot2 library[108] in RStudio software.

(Supplementary Fig. 4). From 05 to 07 December, the inflowing air originated from the mid-latitudes of the Pacific Ocean and entered the continent before taking an anticyclonic turn. In contrast, on 08 and 09 December, the air masses followed a continental path, originating five days earlier from the central region of Brazil. Finally, in this event, the influence of vertical thermal advection on temperature variations was relatively less than that of the other two terms.

To further analyse the process related to the heatwave, we utilise the analogue technique to assess the contribution of three factors to increasing TX anomalies:

Table 1 | Heatwave metrics

Heatwave	Start date	End date	Duration [days]	Mean maximum temperature anomaly [standard deviations]	Spatial coverage [km^2]
Pacific Anticyclone (PAHW)	02 Dec 2022	15 Dec 2022	14	2.7	2,361,077
Multiple Forcings (MFHW)	04 Jan 2023	10 Jan 2023	7	2.7	1,709,794
Transient Anticyclone (TAHW)	03 Feb 2023	15 Feb 2023	13	2.9	2,011,079
Atlantic Anticyclone (AAHW)	07 Mar 2023	23 Mar 2023	17	2.8	1,610,111

Each heatwave is characterised by its date of occurrence, duration, intensity, and spatial extent.

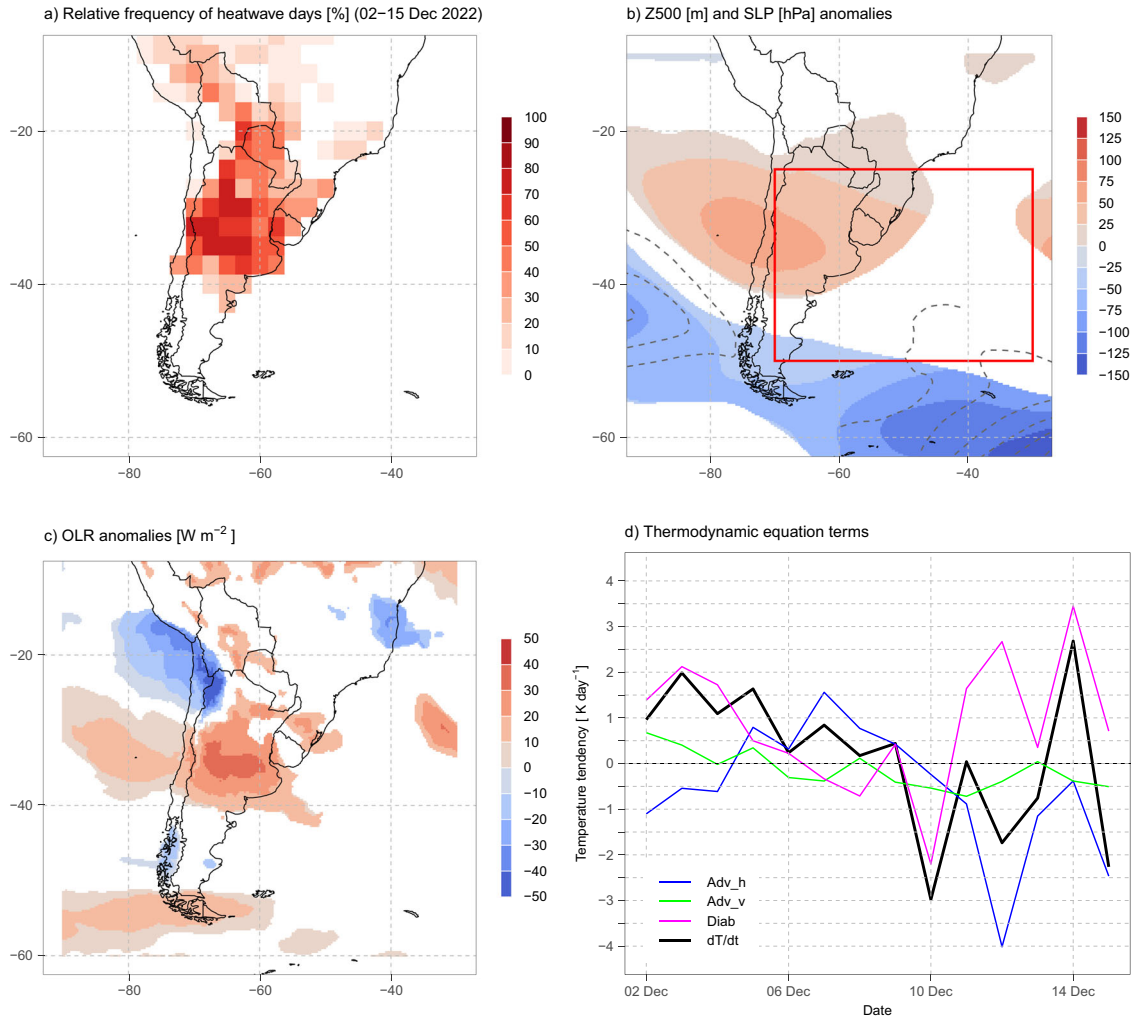

Fig. 2 | Synoptic and thermodynamic conditions during the Pacific Anticyclone Heatwave (PAHW). a Relative frequency of heatwave days from 02 December to 15 December. **b** Composite of geopotential height anomalies at 500hPa (Z500) [m, shading] and sea level pressure anomalies (SLP) [hPa, contours]. **c** Composites of Outgoing Longwave Radiation (OLR) anomalies [W m^{-2}]. **d** Temporal evolution of the 1000-850hPa thermodynamic equation terms [K day^{-1}, Eqs. (1)–(3)] in the region shown in Fig. 1a. For composites, only anomalies significantly different from zero at 10% according to a Student's t-test are shown. Climatology 1981–2010. The red box indicates the area used to obtain atmospheric circulation analogues. *Credit line: The maps were created by the first author using the ggplot2 library[108] in RStudio software.

a. the influence of the mid-level atmospheric circulation by comparing TX under constrained and random flow in the new world (Eq. (4)),
b. the impact of climate change by comparing TX between the new and old world under constrained flow patterns (Eq. (5)), and
c. the amplification of TX anomalies due to soil moisture deficits by contrasting dry and wet soil moisture conditions under constrained flow (Eq. (6)).

For each comparison, the two-sample Kolmogorov-Smirnov test revealed significant differences in the TX anomalies (see Section "Flow Analogue method"). Therefore, TX anomalies obtained from the circulation analogues differ significantly from those obtained from the random flow. Additionally, a significant increase in TX anomalies is observed when comparing the new world to the old one. Similarly, there is a significant amplification of TX on dry soils compared to wet soils. The latter statement responds to the surface energy balance. On dry soils, SHFs are increased at the expense of latent heat fluxes due to limited water availability[25]. Conversely, the opposite occurs on wet soils.

Figure 3a shows that random circulation patterns lead to a wide range of TX anomalies over north-central Argentina. In contrast, circulation

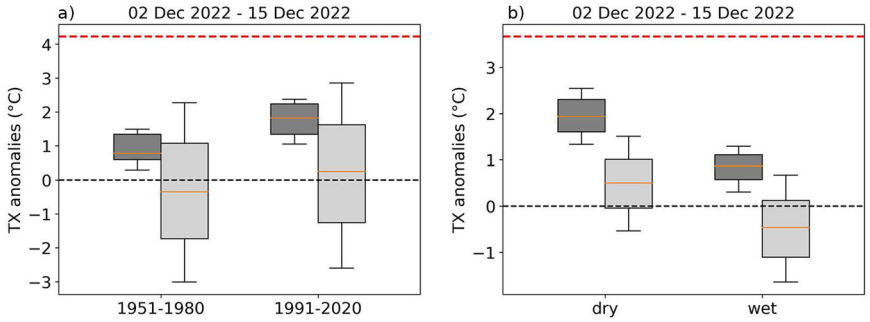

Fig. 3 | Flow analogue reconstruction of maximum temperature anomalies for the Pacific Anticyclone Heatwave (PAHW). Flow conditioned reconstructions from daily analogues of Z500 (dark grey boxes) and random (light grey boxes) distributions of the mean TX anomalies at 2 m over the region shown in Fig. 1a for the PAHW. **a** Reconstructions for the old and new world analogues, (**b**) and preceded by dry and wet conditions. Red dashed lines represent the mean maximum temperature for the event in the region indicated by the green rectangle in Fig. 1a. The difference between the two panels is due to the detrending of temperatures in the wet-dry worlds (panel **b**). The boxes represent the interquartile range and the line inside the box represents the median. The whiskers extend ±1.5 times the interquartile range.

patterns aligned with PAHW analogues consistently result in higher temperatures in the region, with an approximate increase of ~+1.3 °C in the new climate compared to the median TX under random flow conditions (Fig. 3a and Eq. (4), $\Delta\widetilde{TX}_c$ for PAHW). Furthermore, when comparing the new world with the old one (Fig. 3a and Eq. (5), $\Delta\widetilde{TX}_{cc}$), it becomes evident that this constrained flow is associated with a more pronounced warming effect in recent decades, accounting for ~+1 °C greater warming than observed in the old world, primarily attributed to the influence of climate change (although other processes such as changes in land use or aerosols may also be influencing).

Soil desiccation also significantly amplified the TX anomalies during PAHW in northern and central Argentina by playing an important role in enhancing the warm conditions through the soil moisture-atmosphere feedback[25]. Flow patterns, similar to those recorded during PAHW, tend to produce increased anomalies when preceded by dry conditions (Fig. 3b). In other words, dry conditions correspond to TX anomalies of ~+1 °C higher than those obtained with wet soils for a similar atmospheric circulation (Fig. 3b and Eq. (6), $\Delta\widetilde{TX}_{sm}$ for PAHW). This temperature response is representative of a hotspot of land surface-atmosphere coupling, showing how soil moisture constrains evaporation and triggers higher temperatures[25,31]. Furthermore, this soil moisture-temperature coupling can manifest even with random atmospheric flow circulations since positive TX anomalies are more likely to occur under regional drying conditions than when soils are wet.

In summary, our analysis of PAHW reveals that the three factors studied using the analogue technique were important in increasing TX anomalies, each contributing ~+1 °C.

Multiple forcings heatwave (MFHW)

MFHW lasted for one week in early January. As reported by the SMN[6] and depicted in Fig. 4a, this event stood out for its large extension, particularly affecting southern and central Argentina. An anticyclogenesis event occurred in the Argentine Sea, resulting in a high-pressure system over Patagonia (Fig. 4b). Simultaneously, the SACZ was active, as indicated by the Outgoing Longwave Radiation (OLR) anomalies (Fig. 4c and Supplementary Table 1). The enhanced convection over Brazil was associated with a compensatory subsidence branch and the suppression of convection over south-eastern South America[15]. As a result, the highest positive SHF anomalies were observed in central and northern Argentina during this event (Supplementary Fig. 3b).

The Z500 configuration led to an intensification of the polar front jet (PFJ) and a weakening of the subtropical jet (Fig. 4d). This intensification of the westerly belt around 60°S confined cold air to higher latitudes, which hindered the progression of cold fronts into the mid-latitudes. A previous study has identified this jet configuration as a contributing factor to warm TX anomalies during the summer[40]. Among all the heatwave events analysed in this study, MFHW exhibited the highest frequency of days with zonal wind intensification at high latitudes and weakening at subtropical latitudes (Supplementary Table 1).

A closer examination of the thermodynamic equation terms averaged over the Patagonian region (Supplementary Fig. 5b) reveals that diabatic processes were the primary drivers of the diurnal temperature variations during the first half of the event, while horizontal advection dominated the second half (Fig. 4e). This behaviour is a consequence of the location of the anticyclonic system. Initially, the centre of the high-pressure system was located over Patagonia, which promoted clear skies and radiative heating, contributing to the diabatic term. Moreover, on the first day of the event, the subsidence linked to this pressure system also contributed to the warming (as seen in the vertical temperature advection term). In the following days, the anticyclone shifted slightly eastwards, with its centre over the Argentinean Sea. This shift facilitated the horizontal warm advection due to the northerly flow. On the last day of the event, the anticyclone weakened, and temperatures began to decrease.

For this MFHW, the analogue method is implemented in the Patagonian region (with an analogue search region depicted in Supplementary Fig. 5a and a TX reconstruction illustrated in Supplementary Fig. 5b). The flow analogues show that this anticyclonic circulation is always associated with positive TX anomalies in southern Argentina and is significantly different from the random circulation (Fig. 5a). Furthermore, climate change plays an outstanding role in the intensification of TX anomalies under a constrained circulation, as an increase of ~+1.2 °C (Fig. 5a and Eq. (5), $\Delta\widetilde{TX}_{cc}$ for MFHW) is observed relative to the old world.

Argentine Patagonia is a semi-arid region and, therefore, has a weaker soil-atmosphere coupling than north-eastern Argentina[25]. Nevertheless, Fig. 5b shows evidence of this coupling in the warm season in Patagonia because, regardless of the atmospheric circulation, significant differences are found in the empirical distributions of TX anomalies under different soil moisture conditions. In this event, the prevailing anticyclonic circulation over Patagonia inhibited precipitation in the region and generated negative soil moisture anomalies during the heatwave (Supplementary Fig. 5c). Furthermore, the mean soil moisture anomalies in the region were below the 33rd percentile of the climatological distribution in the 15 days before MFHW. Consequently, there was a contribution of dry soil conditions to the amplification of the warm TX anomalies by ~+0.7 °C during the event (compared to wet soil under constrained circulation, $\Delta\widetilde{TX}_{sm}$).

Therefore, among the three factors analysed using the analogue technique, the atmospheric circulation had the greatest impact on increasing the median TX distributions. This conclusion is based on the comparisons of constrained and random circulation medians, which revealed temperature differences of ~+2 °C in the new world (Fig. 5a and Eq. (4), $\Delta\widetilde{TX}_c$ for MFHW).

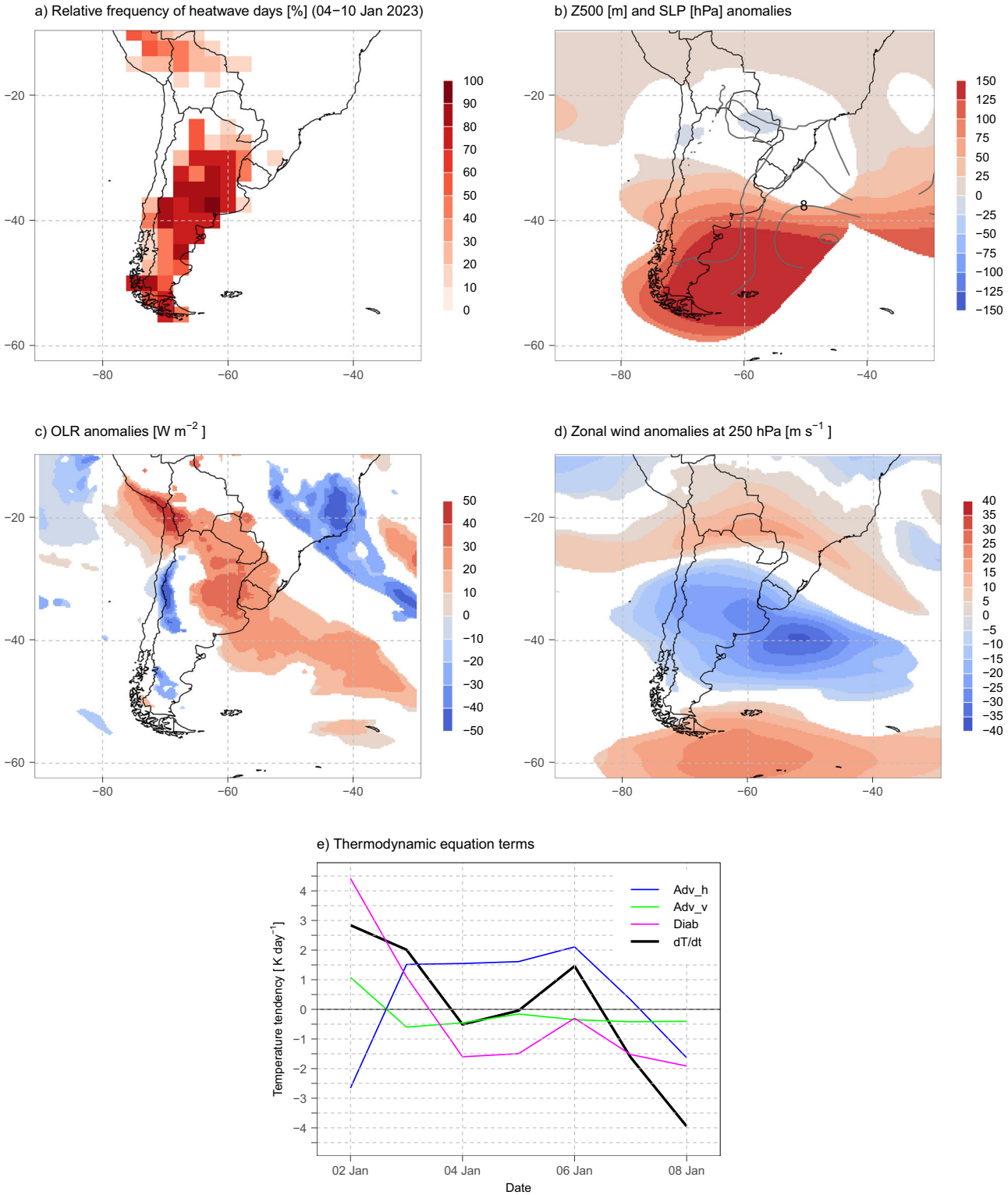

Fig. 4 | Synoptic and thermodynamic conditions during the Multiple Forcings Heatwave (MFHW). a Relative frequency of heatwave days from 04 January to 10 January. **b** Composite of Z500 [m, shading] and SLP anomalies [hPa, contours]. **c** Composites of OLR anomalies [W m^{-2}]. **d** Composite of zonal wind anomalies at 250hPa [m s^{-1}]. **e** Temporal evolution of the 1000-850hPa thermodynamic equation terms [K day^{-1}, Eqs. (1)–(3)] in Patagonia (southern Argentina and Chile). For composites, only anomalies significantly different from zero at 10%, according to a Student's t-test, are shown. Climatology 1981–2010. *Credit line: The maps were created by the first author using the ggplot2 library[108] in RStudio software.

Transient anticyclone heatwave (TAHW)

TAHW started in southern Argentina on 03 February and gradually moved northwards, eventually affecting the entire country (Fig. 6a). However, due to its non-stationary nature, the frequency of heatwave days between 03 and 15 February does not show a high peak at any specific grid point, although local maxima are observed in the eastern region (Supplementary Fig. 6). Moreover, due to its characteristics, the composite analysis during TAHW leads to a loss of atmospheric circulation details. Therefore, Fig. 6b illustrates

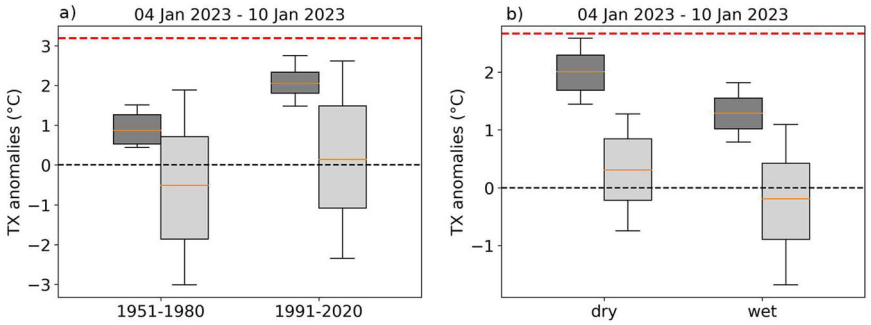

Fig. 5 | Flow analogue reconstruction of maximum temperature anomalies for the Multiple Forcings Heatwave (MFHW). As Fig. 3 but over the Patagonian region shown in Supplementary Fig. 5 and for MFHW. **a** Reconstructions for the old and new world analogues, (**b**) and preceded by dry and wet conditions.

the daily evolution of the Z500 anomalies, providing a better understanding of the relationship between the region affected by TAHW and the anticyclonic anomalies. A strong correspondence between the two is observed when comparing Fig. 6a, b. On 03 February, the event began in Patagonia, where an anticyclonic centre was observed. The system then moved northeastward and weakened towards 07 February, when a ridge formed over Argentina. The next day, an anticyclonic centre began to develop over the Argentine Sea, allowing the area of high pressure to extend back towards Patagonia. Over the following days, this anticyclonic system intensified and gradually moved eastward. Finally, TAHW ended in an intense cyclogenesis over the Argentine Sea. This system caused a cold front to advance over the country, resulting in cold horizontal advection and a sudden drop in temperature (Supplementary Fig. 7). On 16 February, the spatial mean of TX in central Argentina was ~8 °C below average.

The analysis of the thermodynamic equation highlights the importance of the diabatic term in explaining the daily temperature variations in the central and northern regions of the country (Fig. 6c). During the first days of February, this term played a crucial role in warming the region. However, its variability increased from 07 February onwards. Conversely, the horizontal advection of temperature contributed to cooling at the beginning and the end of the event, with only two days showing a warming influence. Finally, the vertical advection of temperature was also slightly more relevant during the early stages of the event, although it contributed less than 1 °C to the temperature tendency.

Analogues are again used to assess the influence of atmospheric circulation, climate change, and drought. The search for circulation analogues narrows the range of variability of the reconstructed temperatures, revealing an association with slightly warm anomalies (about half a degree warmer in the new world compared to the 1951–1980 period). However, it should be noted that this reconstructed temperature differs more from the observed temperature (red dashed line in Fig. 7a) than for the other heatwaves analysed. This may suggest that the circulation plays a less important role than in the other events. Nevertheless, another hypothesis is that the transient characteristics of this heatwave make it difficult to adequately represent the event using the analogue technique, since the methodology considers a fixed domain that does not capture the meridional displacement of the high-pressure system.

Looking at circulation analogues constrained to soil moisture conditions, we observed that drought plays a key role in generating positive TX anomalies in north-central Argentina, contributing ~+1 °C (Fig. 7b and Eq. (6), $\Delta\widetilde{TX}_{sm}$ for TAHW) to the anomalies (Fig. 6b). Conversely, temperature anomalies close to 0 °C are obtained with the same circulation patterns but under wet soil moisture conditions. Thus, soil moisture conditions exerted a stronger influence on TX than atmospheric circulation analogues, which contributed only a few tenths of a degree to the temperature increase.

Atlantic anticyclone heatwave (AAHW)

In March, the last major weather event of the season occurred, mainly affecting central Argentina (Fig. 8a and SMN[3]). This event was characterised by the persistence of an anticyclonic anomaly in Z500, located in the South Atlantic Ocean (Fig. 8b). Furthermore, a cyclonic anomaly centre was observed at higher latitudes, which contributed to an increased mid-latitude horizontal pressure gradient and strengthened the PFJ (Supplementary Fig. 8). As previously mentioned, this favoured warm conditions in Argentina[40].

OLR anomalies indicate that clear skies were favoured over north-central Argentina (Fig. 8c), favouring positive SHF anomalies (Supplementary Fig. 3d). Convection was also inhibited in the SACZ region (Supplementary Table 1). During the inactive phase of the SACZ, heat and moisture are transported from north-western to south-eastern South America by a strong north-south flow driven by the SALLJ[41,42]. The day before SALLJ events reach north-central Argentina, the north-western region of the country experiences high SHFs, low latent heat fluxes, low specific humidity, and warm surface air temperatures due to dry soil moisture. These conditions are conducive to the development of a surface thermal low[43]. The trajectories of the air parcels reaching the central part of the country (64°W-31°S) at 850hPa on 10 and 11 March presented their origin from north-western South America, following the Andes Mountain range (Supplementary Fig. 9). In the following days, they tended to move from positions a little further north-east but maintained a continental path. Therefore, during this event, the largest moisture transports from the Amazon basin to northern and central Argentina were recorded (Supplementary Fig. 10). Under these conditions, on 11 March, a new historical TX record was set for March in Buenos Aires in 117 years of records[44].

During the initial phase of the event (until 16 March), a persistent warm horizontal advection was generally counterbalanced by cold vertical advection (Fig. 8d). Consequently, the daily temperature variations mainly corresponded to changes in the diabatic heat term. It is worth noting, however, that an exception to this pattern occurred on 11 March, when all three terms of the thermodynamic equation contributed to the warming, resulting in a temperature increase of 2 °C compared to the previous day.

In the second half of the event, the diabatic term generally exhibited an opposite influence than the other two terms. However, it was the combined effect of the two advective terms that dominated the temperature changes, inducing cooling during this period. On 20 March, the cold horizontal advection was particularly pronounced. The back-trajectories for this day indicated differences between the members of the Global Forecast System ensemble used to obtain them (Supplementary Fig. 9). While some ensemble members indicated a southerly origin, others suggested a north-easterly origin. A stronger contribution of the southern flow and a larger oceanic path could have influenced the temperature decrease. Towards the end of AAHW event, the trajectories returned to a continental path from central Brazil, and therefore, warm advection predominated in central and northern Argentina.

Analyses of the atmospheric circulation analogues during AAHW reveal that the constrained circulation results in TX anomalies of ~+1.9 °C warmer than the random circulation fields in the new world (Fig. 9a and Eq. (4), $\Delta\widetilde{TX}_c$ for AAHW). In contrast, the random circulation often exhibits negative TX anomalies. Therefore, the presence of an anticyclonic system over the South Atlantic was critical for the occurrence of this event. Comparing the old and new world analogues, we find that the current global warming conditions have contributed to a warming of ~+0.8 °C (Fig. 9a and

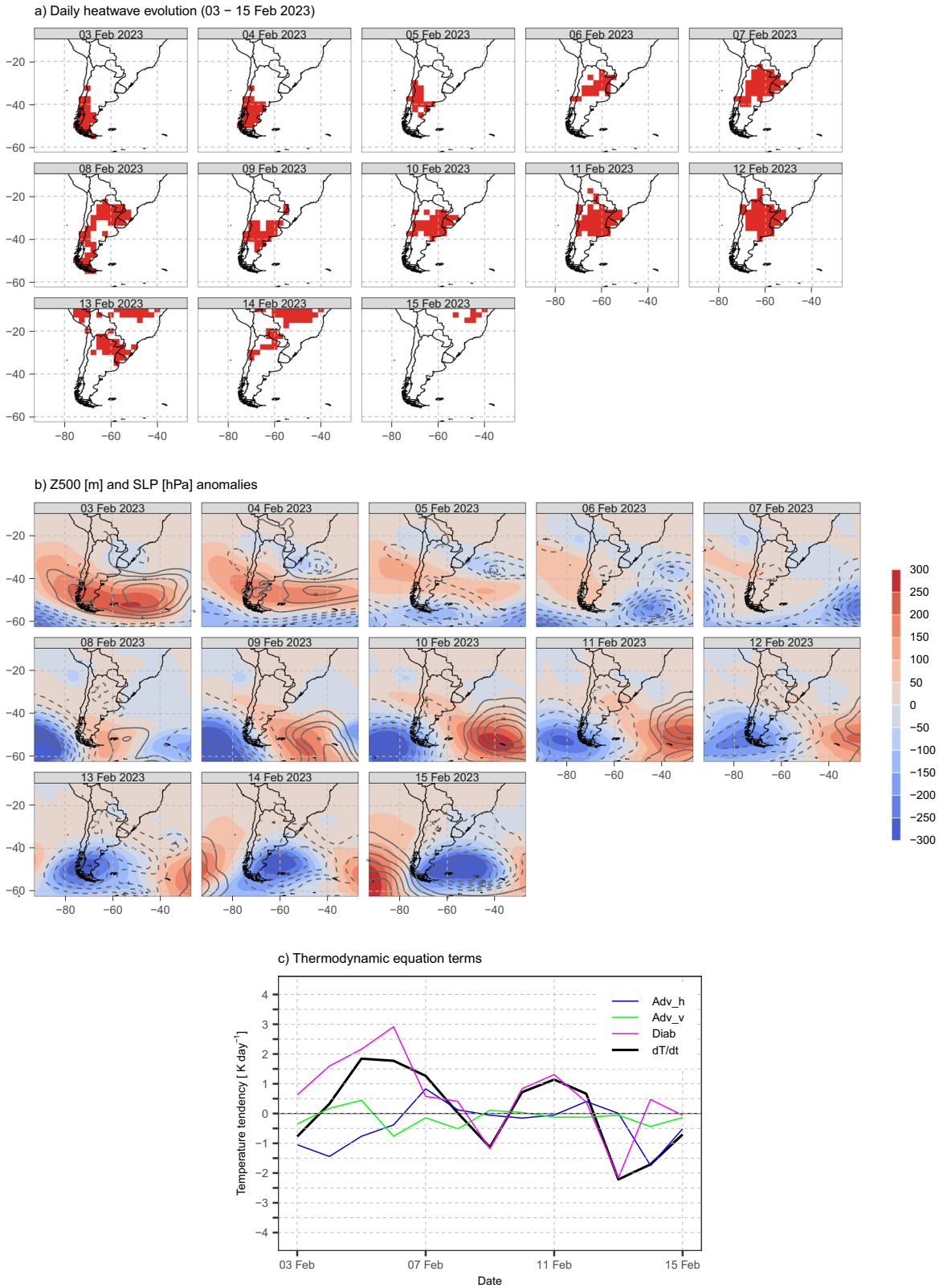

Fig. 6 | Synoptic and thermodynamic conditions during the Transient Anticyclone Heatwave (TAHW). a Heatwave location for each day. **b** Daily Z500 [m, shading] and SLP anomalies [hPa, contours]. **c** Temporal evolution of the 1000-850hPa thermodynamic equation terms [K day^{-1}, Eqs. (1)–(3)] in the region shown in Fig. 1a. *Credit line: The maps were created by the first author using the ggplot2 library[108] in RStudio software.

Eq. (5), $\Delta\widetilde{TX}_{cc}$ for AAHW). Furthermore, we observe that when this circulation coincides with wet conditions, it results in TX anomalies of ~+1 °C. Conversely, during periods of dry conditions, the TX anomalies tend to surpass +2 °C (Fig. 9b). Therefore, the difference in TX anomalies between dry and wet soils exceeds +1 °C (Fig. 9b and Eq. (6), $\Delta\widetilde{TX}_{sm}$ for AAHW). We also note that detrended TX anomalies can be reconstructed very closely to those recorded during the event under flow analogues and low soil moisture conditions.

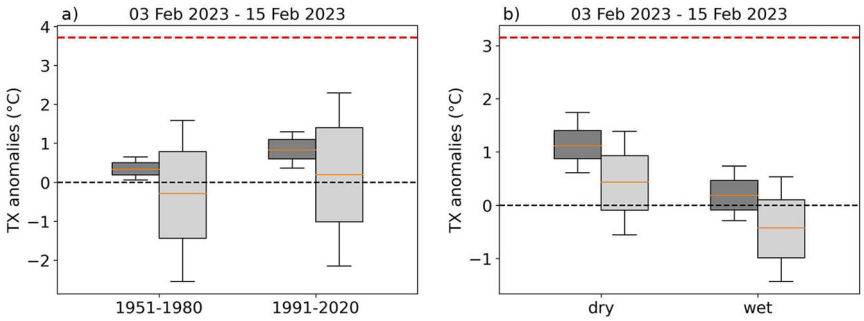

Fig. 7 | Flow analogue reconstruction of maximum temperature anomalies for the Transient Anticyclone Heatwave (TAHW). As Fig. 3 for TAHW. **a** Reconstructions for the old and new world analogues, (**b**) and preceded by dry and wet conditions.

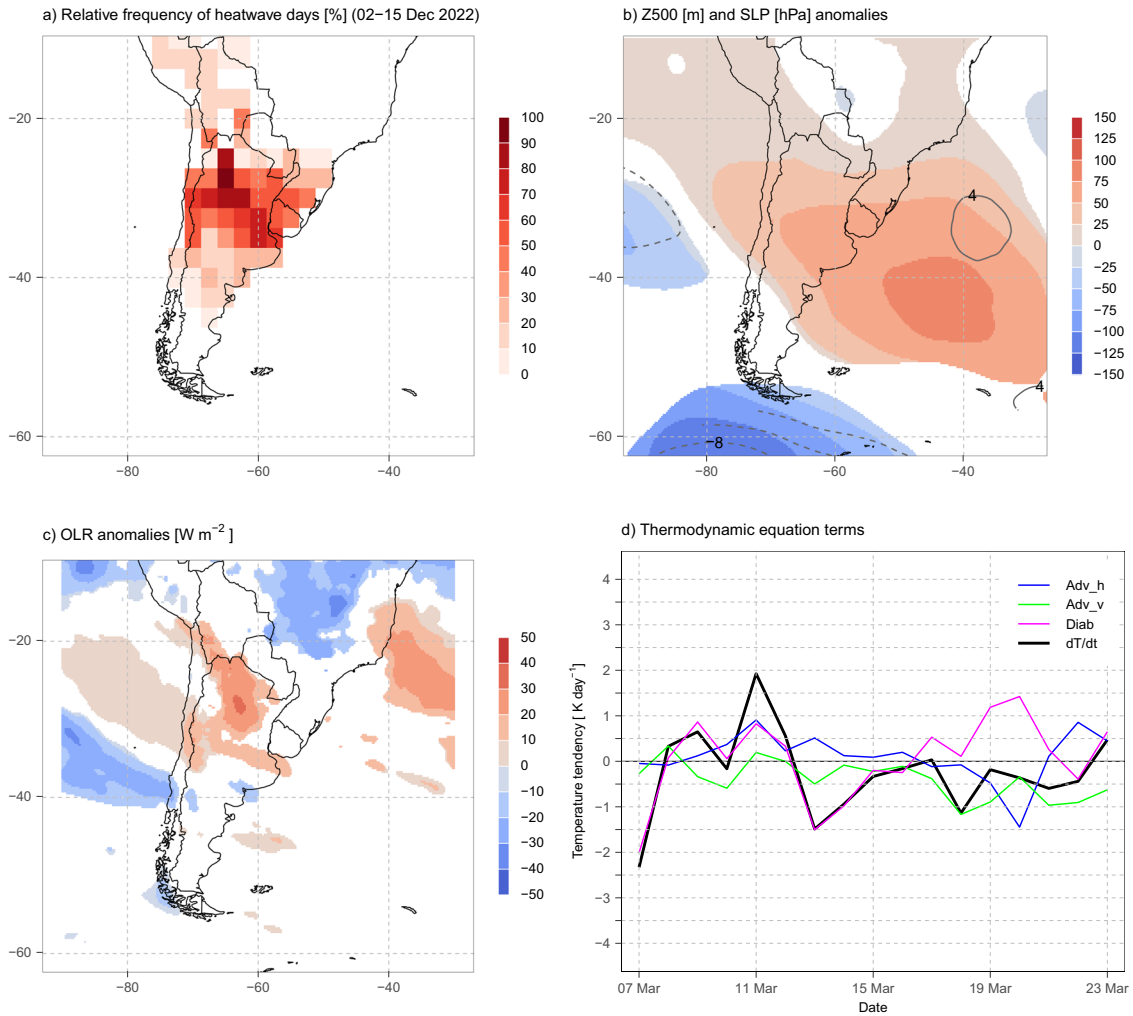

Fig. 8 | Synoptic and thermodynamic conditions during the Atlantic Anticyclone Heatwave (AAHW). a Relative frequency of heat wave days from 07 March to 23 March. **b** Composite of Z500 [m, shading] and SLP anomalies [hPa, contours]. **c** Composites of OLR anomalies [W m^{-2}]. **d** Temporal evolution of the 1000-850hPa thermodynamic equation terms [K day^{-1}, Eqs. (1)–(3)] in the region shown in Fig. 1a. For composites, only anomalies significantly different from zero at 10%, according to a Student's t-test, are shown. Climatology 1981–2010. *Credit line: The maps were created by the first author using the ggplot2 library[108] in RStudio software.

For AAHW, the increase in TX anomalies was attributed to atmospheric circulation, global warming, and soil moisture conditions (Table 2). However, the main factor contributing to the warming of approximately +1.9 °C with respect to the random circulation in the new world was the presence of an anticyclonic centre in the Atlantic (Eq. 4, $\Delta\widetilde{TX}_c$).

Dynamical processes associated with the heatwave events

A common and characteristic feature of all the heatwave events was the presence of a mid-level anticyclonic system, which contributed significantly to the occurrence of warm TX anomalies in Argentina. Extensive previous research has consistently shown that anticyclonic systems play a relevant role in promoting the formation and maintenance of heatwaves globally[8–10,13,45–49]. Furthermore, Suli et al.[13] found that extreme hot events in southern South America are generally associated with quasi-stationary high-pressure systems. In this regard, three of the four events analysed here displayed this characteristic circulation. The only exception was TAHW, which was linked to the advance of a transient high-pressure system moving from Patagonia to northern Argentina.

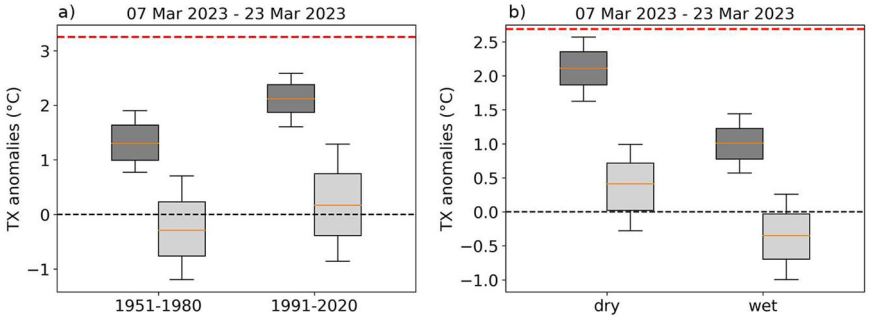

Fig. 9 | Flow analogue reconstruction of maximum temperature anomalies for the Atlantic Anticyclone Heatwave (AAHW). As Fig. 3 for AAHW. **a** Reconstructions for the old and new world analogues, (**b**) and preceded by dry and wet conditions.

Table 2 | Summary of the features and contributions of each heatwave

Heatwave	Main circulation features	Main thermodynamic term	Analogue circulation contribution (Eq. (4), $\triangle\widetilde{TX}_c$)	Analogue global warming contribution (Eq. (5), $\triangle\widetilde{TX}_{cc}$)	Analogue soil moisture contribution (Eq. (6), $\triangle\widetilde{TX}_{sm}$)
PAHW	Pacific anticyclone	Diabatic	~ 1.3 °C	~1 °C	~1.1 °C
MFHW	Central-Eastern Argentina → SACZ Patagonia → Anticyclone	First half → Diabatic Second half → Horizontal advection	~2 °C	~1.2 °C	~0.7 °C
TAHW	Transient Anticyclone	Diabatic	~0.4 °C	~0.5 °C	~1 °C
AAHW	Atlantic Anticyclone	First half → Diabatic Second half → Horizontal and vertical advection	~1.9 °C	~0.8 °C	~1.2 °C

Quantification of the different factors involved in heatwaves from the different analogue exercises.

Among the events with a quasi-stationary anticyclone, the location of the systems was different. PAHW featured a dipole of Z500 anomalies in the South Pacific, which has previously been associated with heatwaves in central Chile[13,14]. Heatwaves of this configuration are typically rare and short-lived, lasting on average about 3.5 days[13]. However, the December 2022 PAHW was remarkably longer than the average, lasting more than 10 days. On the other hand, MFHW and AAHW exhibited an extratropical high-pressure system similar to those identified by Suli et al.[13] for the heatwave occurrences in Patagonia and central Argentina, respectively. The anticyclonic system over extratropical latitudes acted as an atmospheric block, disrupting the usual eastward propagation of pressure systems, and contributing to the prolonged duration of the events. Moreover, this atmospheric block promoted the suppression of the subtropical jet and the intensification and southward shift of the PFJ, which could have contributed to the enhanced warming in Argentina by reducing the frequency of cold frontal passages[40].

In addition to the mid-level circulation, some events exhibited other dynamical processes. A noteworthy distinction among them was the activity of the SACZ (Supplementary Table 1). Previous research has emphasised the importance of the SACZ in heatwave evolution in subtropical South America, with over 70% of events in the region being associated with an active SACZ[16]. In a case study of the December 2013 heatwave, Alvarez et al.[16] highlight that the intensified SACZ contributed to the occurrence of the event, which affected central and northern Argentina. Another study shows that two-thirds of heatwave events in south-eastern Patagonia are associated with convective conditions in the SACZ[50]. During the extended summer of 2022/23, we observed that the active SACZ played a smaller role than expected, according to previous studies, as only the January MFHW showed persistent intensified convection in central and south-eastern Brazil. This limited impact of the SACZ may be attributed to several factors influencing its intra-seasonal variability, such as ENSO[51,52], local sea surface temperature conditions[52,53], or the Madden-Jullian oscillation (MJO)[54,55]. Although the La Niña phase tends to favour an increased occurrence of an active SACZ[51,52], the other drivers could have acted to prevent active SACZ events. In this sense, according to the Brazilian National Institute of Meteorology[56], no active SACZ events were recorded in February and March 2023. During the AAHW event in March, convective activity in the SACZ region was strongly inhibited, favouring the inflow of air masses from the Amazon towards north-central Argentina, driven by an intense meridional component associated with the SALLJ[41,57,58]. Thus, the AAHW recorded the strongest moisture transport among all the events (Supplementary Fig. 10).

Intra-seasonal variability, represented by the MJO, did not greatly contribute to the amplification of TX during these heatwave events. In fact, on some days, it may have even facilitated a decrease in temperatures. Warm anomalies over the extratropical part of the continent are associated with phases 6 to 1 of the MJO in DJF[59]. During PAHW, the MJO was only active in phase 4 between 8 and 12 December, as reported by the Australian Bureau of Meteorology (http://www.bom.gov.au/climate/mjo/, accessed in January 2024). This phase is related to cold anomalies in central-western Argentina and northern Patagonia, which may have contributed to a decrease in temperature in these regions. On the other hand, MFHW was supported by an active MJO in phase 7 only on the first day of the event and was inactive on the other days. In TAHW, the MJO was active on all days of the event, progressing between phases 4 and 6, which generally favoured cooling in many heatwave-affected regions. Finally, the last event of the season occurred in March when the relationship between the MJO and temperatures over Argentina is not significant[59]. Therefore, although the MJO was active, it would not have influenced TX during AAHW.

Interannual variability plays a crucial role in modulating synoptic and intra-seasonal variability in South America during summer[60]. Therefore, it is necessary to analyse the impact of the La Niña event on the extraordinary 2022/23 warm season. In extratropical latitudes, the connection between ENSO and atmospheric circulation anomalies is generated by stationary Rossby wave patterns, which are triggered by anomalous convection over the tropical Pacific[21,61]. Supplementary Fig. 11 displays the NDJFM 2022/23 Rossby wave propagating over the South Pacific Ocean and reaching the South Atlantic Ocean, where anticyclonic anomalies and warm sea surface temperatures (SST) were favoured. This atmospheric circulation reduces the cyclone density over southern South America[62], thus promoting the

increased frequency of anticyclonic conditions over Argentina, which are necessary for heatwave events. Consistently, Collazo et al.[63] have shown that during the warm season, La Niña is the ENSO phase that records the highest number of compound dry-hot events in extratropical South America. On the other hand, the La Niña phase also reduces the frequency and intensity of the SALLJ and the associated moisture transport from the Amazon basin to the mid-latitudes[64,65]. Therefore, the SALLJ mechanism only made a noteworthy contribution during the last heatwave of the season (Supplementary Fig. 10), which coincided with the decline of the La Niña event.

Another important aspect that emerges from Supplementary Fig. 11 is the presence of warm SST anomalies in the southwest Atlantic. Previous research has shown that this SST pattern usually leads to positive air temperature anomalies extending across most of eastern South America[66]. For instance, in January 2022, this SST configuration was linked to a heatwave in south-eastern South America[49]. Moreover, the SACZ tends to weaken under these SST conditions, leading to a significant reduction in cloud cover and precipitation[66].

Finally, it should be noted that the modulation exerted by La Niña on the South American climate during the warm season of 2022/23 may have been amplified by decadal variability, as the Pacific Decadal Oscillation[67] was also in its negative phase[68]. When both modes of variability are in their cold phase, further weakening of the SALLJ and enhanced drying has been observed over south-eastern South America during the warm season[21,69,70].

Thermodynamical processes associated with the heatwave events

All four case studies analysed share a common factor: the diabatic heat term substantially influences the daily temperature variations in the near-surface layer. This term is a complex variable that encompasses several processes, including solar and terrestrial radiation, latent and SHF, and turbulent and convective mixing[71,72]. Since multiple processes are involved, the analysis presented here cannot identify which is dominant. Nevertheless, according to recent research by Schielicke and Pfahl[72], diabatic changes in near-surface air temperature are mainly driven by SHF, which is strongest over dry soils. Furthermore, Röthlisberger and Papritz[73] have quantified the importance of the processes involved in the thermodynamic equation leading to atmospheric heat extremes on a global scale. Consistent with our findings, they find that the diabatic term plays a crucial role in the occurrence of extreme temperatures in north-western and central Argentina.

The influence of horizontal temperature advection in the thermodynamic equation was more variable among the events. It was a relevant contributor for a few isolated days in PAHW, MFHW and AAHW. The highest temperature increases associated with this term were observed when the air mass moving towards central Argentina originated from the Amazon region and followed a continental trajectory. Finally, the vertical temperature advection term generally contributed less than the other terms of the thermodynamic equation in all heatwaves analysed. Conversely, for the January 2022 heatwave in southern South America, Zhang and Xie[49] found that the vertical advection term was the most relevant, followed by diabatic heating. Nevertheless, there is a crucial distinction between our analysis and that of Zhang and Xie[49]. The former only estimates the thermodynamic equation terms at the 850hPa level. However, we evaluate the average in the 1000-850hPa layer to capture better the surface impact on the atmospheric boundary layer. This could explain why we find a higher contribution of the diabatic term to the temperature tendencies. Moreover, as mentioned in the Methods section, vertical motions in the lower levels of the atmosphere are generally of limited magnitude. Consequently, the vertical advection of temperature usually had a minimal influence on the temperature variations of the studied heatwave events.

Global warming and soil condition contribution

The flow analogue technique has been widely used to attribute extreme events[47,74–78]. In our research, we apply this methodology to discern the influence of mid-level atmospheric circulation, soil moisture content and global warming on the occurrence of heatwaves. Each of these factors plays a crucial role in explaining the temperature levels observed during such events. Although the analogue flux approach does not provide an exact reconstruction of the observed temperature anomalies, it facilitates the quantification of the relative impact of each factor (Table 2). For this purpose, we compare the differences between the medians of the probability distributions obtained from various analogue exercises (Eqs. 4–6). Atmospheric circulation emerged as the main driver behind the increase in TX anomalies, except for TAWH due to its transient development. However, it is important to emphasise that for all the heatwaves studied here, the three factors assessed through the flow analogue method favoured warmer conditions. Despite these significant contributions to heatwave intensity, none of them independently explains the observed temperature levels in each event. The combined effect of these factors, interacting in a non-linear way, shapes the observed heatwave intensity in a changing environment, making the reconstruction of the observed temperature anomalies by simply aggregating the individual assessments of each factor inadequate. Additionally, different assumptions are made in each analogue exercise (see Section "Flow Analogue method").

Regardless of the magnitude of the change, we show that the new world is associated with a warmer TX than the old world during all heatwaves, which could be attributed to two key factors: a shift/intensification in circulation patterns leading to amplified heatwave intensities, and/or the influence of the temperature trend resulting from global warming. To determine the role of the changes in the intensity of the atmospheric systems, we repeat the same analogue exercises, focusing on variations in the Euclidean distance metric used to identify analogues (see Section "Flow Analogue method"). Almost no differences are observed between the two worlds, only a slight decrease in the Euclidean distance of MFHW accompanied by an intensification of the Z500 field (Supplementary Fig. 12). These results suggest that the observed change between both worlds is mainly due to the temperature trend in a global warming context. In summary, we have demonstrated that the temperature values recorded for flow analogue days under new-world conditions are highly unlikely under old-world conditions, except for TAHW for which, as mentioned, the analogue methodology has some limitations.

In addition to the heatwave intensity, climate change also modifies the frequency of these events[79]. Traditionally, Argentina experienced an average of four heatwaves per summer between 1977 and 2018. However, during the 2022/23 warm season, a record of ten heatwaves occurred. This high recurrence is part of a wider trend of increasing frequency and persistence of heatwaves in southern South America between 1961–2014, and the pronounced acceleration in the last decade of that period[80–82]. Attributional studies have linked this acceleration to anthropogenic climate change, with high confidence in south-eastern South America and medium confidence in south-western South America[79]. Specifically, the December 2013 heatwave in Argentina was five times more likely in the current world with anthropogenic emissions than in a world without such emissions[83,84]. Additionally, in line with PAHW dates, the record temperatures observed during the December 2022 heatwave were approximately 60 times more likely due to human-caused climate change[1]. Consequently, cities have experienced more consecutive hours of heat stress since the 2000s than in the previous two decades, coupled with a greater persistence of such conditions[85]. The combination of high temperatures, humidity, and clear skies recorded during the 2022/23 heatwaves resulted in large areas of northern and central Argentina experiencing very strong heat stress conditions (Supplementary Fig. 13). Unfortunately, the exposure of the population to these extreme heat events is projected to accelerate further in the future under intermediate and extreme greenhouse gas emission scenarios[63]. Furthermore, the frequency and intensity of heatwaves in Argentina, as well as the number of hot and dry compound events, are projected to increase towards the end of the century under moderate and high emissions scenarios[63,80].

The analogue exercise applied to assess the contribution of soil moisture content highlights the importance of the land-atmosphere coupling in partially explaining the TX anomalies associated with the heatwaves (Table 2, $\widetilde{\Delta TX}_{sm}$). Particularly in south-eastern South America, known as a

hotspot for soil moisture-atmosphere coupling[27,28], temperatures are notably responsive to changes in soil moisture levels. Particularly, PAHW, TAHW, and AAHW exhibited a difference in TX anomalies between the dry and wet analogues of ~+1 °C in central and northern Argentina. This sensitivity was also demonstrated in the 2013/2014 mega-heatwave in south-eastern Brazil, where a strong soil moisture-temperature coupling regime played a pivotal role[34]. Dry soil conditions in coupling regions tend to amplify positive temperature anomalies by reducing latent heat flux and favouring SHF, leading to a deeper, drier, and warmer planetary boundary layer, subsequently reducing cloud cover, and enhancing net solar radiation[25]. The cumulative multi-day memory of the atmospheric boundary layer and the land surface has been identified as a significant factor driving extreme temperatures, notably in the European mega-heatwaves of 2003 and 2010[86]. Consequently, further investigation into the daily evolution of the atmospheric boundary layer during the 2022/23 heatwave events is required in future studies.

Finally, it is important to clarify that other regions with weaker soil-atmosphere coupling may emerge as hotspots when soil moisture increases to an intermediate level (see Fig. 5 in Seneviratne et al.[25] and Diro et al.[87]). This phenomenon was observed during MFHW in the semi-arid Argentine Patagonia when the previously dry soils contributed to warmer anomalies of ~+0.7 °C in southern Argentina (Table 2, $\Delta\widetilde{TX}_{sm}$ for MFHW). Our results demonstrate that varying levels of soil moisture led to distinct TX anomalies, suggesting some coupling between them.

Conclusions

The main objective of this study is to provide a comprehensive analysis of the highly unusual warm season of 2022/23 in Argentina. This season was characterised by an exceptionally high heatwave frequency, with ten events affecting different regions of the country. The seasonal TX anomalies recorded during this period reached historical highs, especially in central Argentina. Remarkably, more than 40% of the days of the season were affected by heatwaves. To identify the influences of synoptic patterns, thermodynamics, soil moisture content, and climate change, our study focuses on the four heatwaves with the largest spatial extent. The main conclusions of this work are listed below:

- Synoptic situation: The presence of anticyclonic anomalies in the mid-level atmosphere proved to be a necessary condition for the occurrence of heatwaves in the 2022/23 warm season. These atmospheric systems led to clear skies and subsidence, which together facilitated the warming. In addition, we observe that 3 out of 4 heatwaves had the presence of a quasi-stationary anticyclone, while the other had a transient system. Moreover, this atmospheric circulation pattern interacted with other processes, such as the SACZ in the MFHW or the SALLJ in the AAHW. In these two events, we also noted that the atmospheric circulation played a fundamental role in the amplification of TX, providing warming of ~+2 °C (compared to what would be obtained by a random circulation under present climate conditions).
- Thermodynamic processes: Diabatic heating processes emerged as the primary drivers of daily-scale temperature changes in the analysed heatwave events. Furthermore, we observed that horizontal advection made its most relevant contribution to daily warming when a tropical air mass entered central and northern Argentina.
- Soil moisture content: All heatwave events were characterised by deficits in soil moisture content, because of the third consecutive year of the La Niña phase. These deficits caused an increase in SHF and an amplification of warming through the strong soil moisture-atmosphere coupling in north-central Argentina. Using the flow-analogue technique, we quantified that the contribution of dry soils to warming relative to wet soils was ~1 °C.
- Interannual variability: The record-breaking drought of 2022/23 in Argentina can be primarily attributed to the triple-dip La Niña event[23,38]. These La Niña occurrences, which promote anticyclonic conditions over central-northern Argentina, have been consistently associated with precipitation deficits and major historical drought[38,88]. Furthermore, Menéndez et al.[29] found that interannual variability of soil moisture can amplify the temperature variability in the southern La Plata Basin during the austral summer months. They also speculate that, due to the impact that ENSO exerts on land surface conditions, the combination of both processes could alter ENSO-induced temperature anomalies in this region.
- Climate change: Further analysis using analogues revealed that global warming in recent decades has contributed to an increase in temperature anomalies between 0.5 and 1.2 °C. In essence, atmospheric circulation patterns, similar to those observed during the events analysed, lead to warmer conditions in the present compared to what would have been observed in the past, mostly due to temperature trends rather than changes in the intensity of weather systems.

Finally, we need to consider whether a summer as extreme as 2022/23 could be repeated in the next few years. We have shown that the extremely high temperatures were the result of a combination of factors. The extreme drought associated with the three-year La Niña period is one factor that has only occurred three times since 1960. However, a recent study by Geng et al.[89] found that consecutive La Niña episodes are likely to become more frequent in the 21st century as a result of climate change. North-eastern Argentina, being a region with a strong ENSO teleconnection and a hotspot of soil-atmosphere interaction, could be particularly sensitive to these changes. Moreover, temperature trends are also expected to continue to accentuate[90]. Our research indicates that this contributes to the intensification of heatwaves by several tenths of a degree. Hence, it is probable that an extended summer comparable to the one evaluated will reoccur in the future, and the country will have to prepare for the consequences in terms of health[91,92], energy[93], and agriculture[94] (the main economic activity in Argentina).

Methods

Data

We use daily mean fields provided by ERA5 reanalysis at 0.25° resolution[95] for southern South America (80-45°W, 60-20°S) during the extended summer (warm season: November – March) of 1950 – 2023. In particular, we employ Z500, the temperature at 2 m, sea level pressure, zonal wind at 250 hPa, surface SHF at 18Z, and OLR to characterise the circulation patterns that triggered the Argentine heatwaves during the extended summer of 2022/23. In addition, we examine the thermodynamic contribution to the daily evolution of heatwaves using the horizontal wind vector, vertical velocity, and potential temperature data between the 1000 – 850 hPa layer. Additionally, we estimate the moisture transport at 850 hPa using the horizontal wind vector and the specific humidity. We also utilise the volume of water in the soil layer 1 ($0-7$ cm) to study the land-atmosphere coupling under dry/humid soil moisture conditions in the region.

Finally, to measure heat stress in outdoor spaces, we employ the Universal Thermal Climate Index bioclimatic index of the ERA5-HEAT product (https://cds.climate.copernicus.eu/cdsapp#!/dataset/derived-utci-historical?tab=overview, accessed in January 2024). This index describes the physiological comfort of the human body under specific meteorological conditions[96]. It is considered one of the most comprehensive indices as it takes into account not only air temperature but also humidity, wind, and radiation[97,98]. The Universal Thermal Climate Index is divided into ten categories, ranging from extreme cold stress to extreme heat stress. Values between 32 °C and 38 °C are associated with strong heat stress, while values between 38 °C and 46 °C are associated with very strong heat stress[98].

Heat waves detection

To identify Argentine summer heatwaves, we apply the semi-Lagrangian algorithm developed by Sánchez-Benítez et al.[37] to daily gridded maximum temperature at 2 m. In contrast to the Eulerian approach (e.g., Bitencourt et al.[99]; Perkins and Alexander[100]; see Barriopedro et al.[8], for a review), which considers heatwaves as isolated local surface spatio-temporal structure of

the events, the semi-Lagrangian perspective analyses the entire temperature field, identifying and tracking the spatio-temporal structure of the events.

The algorithm comprises two phases:

(i) Identification of daily heatwave patterns. For each day, the algorithm detects areas larger than 500,000 km2 (including or excluding oceans) where the maximum temperature at 2 m exceeds the local 90th percentile of the 1981–2010 period, calculated using a 31-day centred window. These spatial patterns may include non-contiguous areas if their distance is less than 750 km.

(ii) Tracking of heatwave events. Two spatial patterns occurring on consecutive days are classified as the same event if they overlap by at least 50% or the distance between their centres is less than 1000 km for any non-null overlap. The latitudinal (longitudinal) centre is defined as the intensity-weighted average latitude (longitude) of all grid points constituting the daily heatwave pattern. The local heatwave intensity is computed as the standardised 2m-temperature anomaly. For the centre's computation, these anomalies have been subsequently multiplied by the cosine of latitude in order to account for spatial changes in areal extent.

A calibration and evaluation of the semi-Lagrangian algorithm was previously performed for the southern South American region. The algorithm's results showed robustness to minor variations in the algorithm's parameters.

Further details of the methodology can be found in Sánchez-Benítez et al.[37,101].

The methodology yields multiple metrics (e.g., mean areal extent, intensity, overlapping, speed, and centre location) that allow us to characterise the heatwave event throughout its life cycle. These include start and end dates, duration (days), and maximum and mean daily metrics computed for the entire life-cycle of the heatwave.

Heat waves characterisation

We characterise the atmospheric circulation during the heatwaves by composites of meteorological fields (Z500, OLR, SHF, etc.) for each heatwave day. Daily anomalies are computed removing the 1981–2010 mean for each calendar day. Statistical significance is evaluated using the t-Student test at a 90% confidence level.

For each heatwave day, we also assess the thermodynamic equation to determine the influence of three major physical forcings on daily temperature tendencies: horizontal advection, vertical advection, and diabatic processes. Daily mean horizontal (Eq. (1)) and vertical (Eq. (2)) advection are determined as:

$$\left(\frac{\Delta T}{\Delta t}\right)_h(\lambda,\phi,t) = -\vec{v}.\nabla_p T \tag{1}$$

$$\left(\frac{\Delta T}{\Delta t}\right)_v(\lambda,\phi,t) = -\omega\frac{T}{\theta}\frac{\partial\theta}{\partial p} \tag{2}$$

where $\vec{v}$ is the horizontal wind, T the temperature, ω the vertical velocity, θ the potential temperature, and (λ, ϕ, t) the latitude, longitude, and time, respectively. These equations are computed from daily mean fields considering the seven pressure levels available in the ERA5 reanalysis (between 1000 – 850 hPa layer) over a given domain of southern South America (10–55°W, 40–25°S). The daily mean temperature rate attributed to additional diabatic processes (e.g., radiative and heat fluxes) is determined as the residual term derived from the temperature tendency equation (Eq. (3)) after considering the effects of the two preceding terms:

$$\left(\frac{\Delta T}{\Delta t}\right)_d(\lambda,\phi,t) = \frac{\Delta T}{\Delta t} - \left(\frac{\Delta T}{\Delta t}\right)_h - \left(\frac{\Delta T}{\Delta t}\right)_v \tag{3}$$

where $\frac{\Delta T}{\Delta t}$ is the daily mean temperature tendency (in $K\ day^{-1}$). It is important to acknowledge that various factors, including sub-grid turbulent mixing, analysis increments, and other numerical errors, can influence the residual term. Hence, the causal attribution of temperatures should be taken with caution, as a composite analysis may not detect all one-directional causal relationships. Finally, it should be noted that the vertical thermal advection term in the lower atmosphere is generally small due to the weak vertical wind speeds near the surface (they usually peak in the middle atmosphere in the non-divergence level[102]).

We also employ the Hybrid Single-Particle Lagrangian Integrated Trajectory (HYSPLIT) model (available at: https://www.ready.noaa.gov/hypub-bin/trajtype.pl) developed at the Air Resource Laboratory of the National Oceanic and Atmospheric Administration (NOAA)[103] to determine the origin of air masses that end in central Argentina (64°W-31°S) at approximately 850 hPa and to establish source-receptor relationships. To achieve this, we apply a 5-day backward trajectory analysis using Global Forecast System ensemble data at 0.25 resolution.

Flow analogue method

The flow analogue methodology is used to analyse the influence of the mid-level atmospheric circulation, the impact of climate change, and soil moisture conditions on the heatwaves. For this purpose, factual and counterfactual universes are defined, representing opposite worlds to contrast the differences in the forcings. For PAHW, TAHW, and AAHW, the search region for flow analogues was defined based on the climatological circulation patterns associated with the occurrence of heatwaves in central and northern Argentina, while for MFHW, the climatological position of the anticyclonic centre associated with the Patagonian heatwaves was taken into account[13].

To analyse the influence of climate change, an approximation through the new-old world is done[77,104], where the period 1991–2020 is used for the present climate and 1951–1980 for the past climate. The difference between these between two different periods was considered as a measure of the changes. However, we must be aware that these differences could be modulated by other processes that we have not considered, such as changes in land use[105] or aerosol concentrations[106]. On the other hand, the influence of soil conditions on temperature anomalies is studied using the 66.6 and 33.3 percentiles of soil moisture anomalies as thresholds to represent the wet and dry worlds, respectively. Days with soil moisture anomalies above (below) the former threshold are considered to correspond to the wet (dry) world. In the soil moisture exercise, we removed the linear monotonic trend (analysed with a Mann-Kendall trend test) to avoid the effects of long-term trends that may complicate the causality of the relationship between soil moisture and temperature[47].

In both exercises, the analogues are sought to have similar synoptic patterns. Similar analyses have been carried out in previous work (see, e.g., Sousa et al.[47]). An analogue vector $a = [a_1, a_2, a_3, \ldots, a_N]$ is computed for each heatwave day. Such analogue days are closer to the target day according to the Euclidean distance for the Z500 anomaly in the region [75–30°W, 60–35°S] for MFHW and [70–30°W, 50–25°S] for the other heatwaves. Furthermore, a window of N_{win} days is considered for each heatwave day, i.e., the search for analogue days is restricted to the interval $[-N_{win}/2, +N_{win}/2]$ of the target day. For each heatwave day, a random analogue is drawn from the N (i.e., it was picked up one a_i from a) to compute the mean value of the simultaneous TX. This procedure is repeated 1000 times to derive the mean analogue distribution of TX. Factors such as the domain size for collecting analogues days or the size of the dataset could influence the performance of the analogue-temperature field reconstruction[78], thus we perform a sensitivity analysis. Values of N_{win} = 42,62,90 and N=15,20,25 are tested and yielded similar results, so N_{win} = 90 and N=25 are chosen. Furthermore, different choices in the spatial domain also produced comparable outcomes.

In order to test whether the dynamics played a significant role in the reconstructed anomalies of the target field, randomly selected days, without any condition on the flow, are retrieved to make the unconditional distribution. In this sense, two seeds are set for the random processes with indistinguishable outcomes. A two-sample Kolmogorov-

Smirnov Test[107] is performed to examine the differences between the new-old world and wet-dry distributions against themselves and against the random distributions used to assess the importance of synoptic circulation in maintaining the heatwave conditions. The null hypothesis states that both samples are drawn from the same distribution, while the alternative hypothesis states that the null hypothesis is false. This test is performed at a significance level of α=0.05. In addition, the anomalies used are calculated with respect to the period 1981–2010 and all variables are detrended for the wet-dry experiment to make them insensitive to the climate change signal.

Finally, we quantify the influence of mid-level atmospheric circulation (Eq. (4)), climate change (Eq. (5)), and soil moisture conditions (Eq. (6)) on TX anomalies:

$$\Delta\widetilde{TX}_c = TX_{constrained\,(91-20)} - TX_{random\,(91-20)} \quad (4)$$

$$\Delta\widetilde{TX}_{cc} = TX_{constrained\,(91-20)} - TX_{constrained\,(51-80)} \quad (5)$$

$$\Delta\widetilde{TX}_{sm} = TX_{constrained\,(dry)} - TX_{constrained\,(wet)} \quad (6)$$

where $\widetilde{\Delta TX}$ is the TX median anomalies increased/decreased for each of the cases (c: circulation, cc: climate change, and sm: soil moisture).

Data availability

All data used in this study is publicly accessible online via the following links: ERA5 reanalysis dataset is available in the Climate Data Store https://cds.climate.copernicus.eu/cdsapp#!/search?type=dataset. NOAA Hysplit https://www.ready.noaa.gov/hypub-bin/trajtype.pl.

Code availability

All codes used in this study are available upon request after publication.

Received: 16 October 2023; Accepted: 11 April 2024;
Published online: 03 May 2024

References

1. Rivera, J. A. et al. 2022 early-summer heatwave in Southern South America: 60 times more likely due to climate change. *Clim. Change* **176**, 102 (2023).
2. Stella, J. L. *Informe Especial Por Persistencia de Calor Extremo y Recurrencia de Olas de Calor En Argentina Desde Noviembre 2022*. http://hdl.handle.net/20.500.12160/2358 (2023).
3. Stella, J. L. *Informe Especial N°10 Por Ola de Calor / Altas Temperaturas Temporada 2022-2023*. http://hdl.handle.net/20.500.12160/2407 (2023).
4. Stella, J. L. *Informe Especial N°2 Por Ola de Calor/Altas Temperaturas Temporada 2022-2023*. http://hdl.handle.net/20.500.12160/2216 (2022).
5. Stella, J. L. *Informe Especial N°3 Por Ola de Calor/Altas Temperaturas Temporada 2022-2023*. http://hdl.handle.net/20.500.12160/2217 (2022).
6. Stella, J. L. *Informe Especial N°5 Por Ola de Calor/Altas Temperaturas Temporada 2022-2023*. http://hdl.handle.net/20.500.12160/2279 (2023).
7. Stella, J. L. *Informe Especial N°8 Por Ola de Calor/Altas Temperaturas Temporada 2022-2023*. http://hdl.handle.net/20.500.12160/2364 (2023).
8. Barriopedro, D., García-Herrera, R., Ordóñez, C., Miralles, D. G. & Salcedo-Sanz, S. Heat waves: Physical understanding and scientific challenges. *Rev. Geophys.* **61**, e2022RG000780 (2023).
9. Geirinhas, J. L., Trigo, R. M., Libonati, R., Coelho, C. A. S. & Palmeira, A. C. Climatic and synoptic characterization of heat waves in Brazil. *Int. J. Climatol.* **38**, 1760–1776 (2018).
10. Sousa, P. M., Trigo, R. M., Barriopedro, D., Soares, P. M. M. & Santos, J. A. European temperature responses to blocking and ridge regional patterns. *Clim. Dyn*. **50**, 457–477 (2018).
11. Wang, P., Tang, J., Wang, S., Dong, X. & Fang, J. Regional heatwaves in china: a cluster analysis. *Clim. Dyn.* **50**, 1901–1917 (2018).
12. Fragkoulidis, G., Wirth, V., Bossmann, P. & Fink, A. H. Linking Northern Hemisphere temperature extremes to Rossby wave packets. *Quart. J. R. Meteorol. Soc.* **144**, 553–566 (2018).
13. Suli, S., Barriopedro, D., García–Herrera, R. & Rusticucci, M. Regionalisation of heat waves in southern South America. *Weather Clim. Extrem*. **40**, 100569 (2023).
14. Demortier, A., Bozkurt, D. & Jacques-Coper, M. Identifying key driving mechanisms of heat waves in central Chile. *Clim. Dyn.* **57**, 2415–2432 (2021).
15. Cerne, S. B. & Vera, C. S. Influence of the intraseasonal variability on heat waves in subtropical South America. *Clim. Dyn.* **36**, 2265–2277 (2011).
16. Alvarez, M. S., Cerne, B., Osman, M. & Vera, C. S. Intraseasonal and low frequency processes contributing to the December 2013 heat wave in Southern South America. *Clim. Dyn.* **53**, 4977–4988 (2019).
17. Cerne, S. B., Vera, C. S. & Liebmann, B. The nature of a heat wave in Eastern Argentina occurring during SALLJEX. *Mon. Weather Rev.* **135**, 1165–1174 (2007).
18. Liebmann, B., Kiladis, G. N., Vera, C. S., Saulo, A. C. & Carvalho, L. M. V. Subseasonal variations of rainfall in south america in the vicinity of the low-level jet east of the Andes and Comparison to Those in the South Atlantic Convergence Zone. *J Clim* **17**, 3829–3842 (2004).
19. McPhaden, M. J., Zebiak, S. E. & Glantz, M. H. ENSO as an integrating concept in earth science. *Science (1979)* **314**, 1740–1745 (2006).
20. Grimm, A. M. & Tedeschi, R. G. ENSO and extreme rainfall events in South America. *J. Clim.* **22**, 1589–1609 (2009).
21. Reboita, M. S. et al. Impacts of teleconnection patterns on South America climate. *Ann. N.Y Acad. Sci.* **1504**, 116–153 (2021).
22. World Meteorological Organization (WMO). *State of the Global Climate 2022*. (2023).
23. Geirinhas, J. L. et al. Combined large-scale tropical and subtropical forcing on the severe 2019–2022 drought in South America. *NPJ Clim. Atmos. Sci.* **6**, 185 (2023).
24. Berg, A. & Sheffield, J. Climate change and drought: the soil moisture perspective. *Curr. Clim. Change Rep.* **4**, 180–191 (2018).
25. Seneviratne, S. I. et al. Investigating soil moisture–climate interactions in a changing climate: A review. *Earth Sci. Rev.* **99**, 125–161 (2010).
26. Jung, M. et al. Recent decline in the global land evapotranspiration trend due to limited moisture supply. *Nature* **467**, 951–954 (2010).
27. Sörensson, A. A. & Menéndez, C. G. Summer soil–precipitation coupling in South America. *Tellus A: Dyn. Meteorol. Oceanogr.* **63**, 56 (2011).
28. Ruscica, R. C., Sörensson, A. A. & Menéndez, C. G. Pathways between soil moisture and precipitation in southeastern South America. *Atmos. Sci. Lett.* **16**, 267–272 (2015).
29. Menéndez, C. G. et al. Temperature variability and soil–atmosphere interaction in South America simulated by two regional climate models. *Clim. Dyn*. **53**, 2919–2930 (2019).
30. Menéndez, C., Zaninelli, P., Carril, A. & Sánchez, E. Hydrological cycle, temperature, and land surface-atmosphere interaction in the La Plata Basin during summer: response to climate change. *Clim. Res.* **68**, 231–241 (2016).
31. Coronato, T. et al. The impact of soil moisture–atmosphere coupling on daily maximum surface temperatures in Southeastern South America. *Clim Dyn* **55**, 2543–2556 (2020).

32. Zaninelli, P. G., Menéndez, C. G., Falco, M., López-Franca, N. & Carril, A. F. Future hydroclimatological changes in South America based on an ensemble of regional climate models. *Clim. Dyn.* **52**, 819–830 (2019).
33. Ruscica, R. C., Menéndez, C. G. & Sörensson, A. A. Land surface-atmosphere interaction in future South American climate using a multi-model ensemble. *Atmos. Sci. Lett.* **17**, 141–147 (2016).
34. Geirinhas, J. L. et al. The influence of soil dry-out on the record-breaking hot 2013/2014 summer in Southeast Brazil. *Sci. Rep.* **12**, 5836 (2022).
35. Libonati, R. et al. Assessing the role of compound drought and heatwave events on unprecedented 2020 wildfires in the Pantanal. *Environ. Res. Lett.* **17**, 015005 (2022).
36. Napoli, C. Di, Pappenberger, F. & Cloke, H. L. Verification of Heat Stress Thresholds for a Health-Based Heat-Wave Definition. *J. Appl. Meteor. Climatol.* **58**, 1177–1194 (2019).
37. Sánchez-Benítez, A., Barriopedro, D. & García-Herrera, R. Tracking Iberian heatwaves from a new perspective. *Weather Clim. Extrem*. **28**, 100238 (2020).
38. Arias, P. A. et al. Interplay between climate change and climate variability: The 2022 drought in Central South America. *Clim. Change* **177**, 6 (2024).
39. Muñoz, A., Jager, D. E., de Moraes, L. & Toreti, A. The 2019–2021 extreme drought episode in La Plata Basin A Joint Report from EC-JRC, CEMADEN, SISSA and WMO. in. https://doi.org/10.2760/773 (2021).
40. Collazo, S., García-Herrera, R. & Barriopedro, D. Summer upper-level jets modulate the response of South American climate to ENSO. *Clim. Dyn*. **62**, 1031–1054 (2024).
41. Gulizia, C., Camilloni, I. & Doyle, M. Identification of the principal patterns of summer moisture transport in South America and their representation by WCRP/CMIP3 global climate models. *Theor. Appl. Climatol.* **112**, 227–241 (2013).
42. Vera, C. et al. The South American low-level jet experiment. *Bull. Am. Meteorol. Soc.* **87**, 63–78 (2006).
43. Yang, Z. & Dominguez, F. Investigating land surface effects on the moisture transport over South America with a moisture tagging model. *J. Clim.* **32**, 6627–6644 (2019).
44. SMN. Marzo extremo: altas temperaturas y récords históricos. https://www.smn.gob.ar/noticias/marzo-extremo-altas-temperaturas-y-r%C3%A9cords-hist%C3%B3ricos#:~:text=El%20s%C3%A1bado%2011%2C%20CABA%20(OCBA,del%207%2F3%2F1952. (2023).
45. de Araújo, G. R. G., Frassoni, A., Sapucci, L. F., Bitencourt, D. & de Brito Neto, F. A. Climatology of heatwaves in South America identified through ERA5 reanalysis data. *Int. J. Climatol.* **42**, 9430–9448 (2022).
46. Marengo, J. A. et al. The heat wave of October 2020 in central South America. *Int. J. Climatol.* **42**, 2281–2298 (2022).
47. Sousa, P. M. et al. Distinct influences of large-scale circulation and regional feedbacks in two exceptional 2019 European heatwaves. *Commun Earth Environ*. **1**, 48 (2020).
48. Zschenderlein, P., Pfahl, S., Wernli, H. & Fink, A. H. A Lagrangian analysis of upper-tropospheric anticyclones associated with heat waves in Europe. *Weather and Climate Dynamics* **1**, 191–206 (2020).
49. Zhang, B. & Xie, Z. Mechanism of the record-breaking heatwave event dynamics in South America in January 2022. *Atmosphere (Basel)* **14**, 326 (2023).
50. Jacques-Coper, M., Brönnimann, S., Martius, O., Vera, C. & Cerne, B. Summer heat waves in southeastern Patagonia: An analysis of the intraseasonal timescale. *Int. J. Climatol.* **36**, 1359–1374 (2016).
51. Sulca, J. C. & da Rocha, R. P. Influence of the coupling south Atlantic convergence zone-El Niño-Southern Oscillation (SACZ-ENSO) on the projected precipitation changes over the Central Andes. *Climate* **9**, 77 (2021).
52. Barreiro, M., Chang, P. & Saravanan, R. Variability of the South Atlantic convergence zone simulated by an atmospheric general circulation model. *J. Clim.* **15**, 745–763 (2002).
53. Jorgetti, T., da Silva Dias, P. L. & de Freitas, E. D. The relationship between South Atlantic SST and SACZ intensity and positioning. *Clim Dyn* **42**, 3077–3086 (2014).
54. Fernandes, L. G. & Grimm, A. M. ENSO modulation of global MJO and its impacts on South America. *J. Clim.* **36**, 7715–7738 (2023).
55. Alvarez, M., Vera, C. & Kiladis, G. MJO Modulating the Activity of the Leading Mode of Intraseasonal Variability in South America. *Atmosphere (Basel)* **8**, 232 (2017).
56. INMET. https://portal.inmet.gov.br/boletinsprog (2023).
57. Herdies, D. L. Moisture budget of the bimodal pattern of the summer circulation over South America. *J. Geophys. Res.* **107**, 8075 (2002).
58. Vera, C. et al. Toward a Unified View of the American Monsoon Systems. *J. Clim.* **19**, 4977–5000 (2006).
59. Alvarez, M. S., Vera, C. S., Kiladis, G. N. & Liebmann, B. Influence of the Madden Julian Oscillation on precipitation and surface air temperature in South America. *Clim. Dyn*. **46**, 245–262 (2016).
60. Grimm, A. M. Interannual climate variability in South America: Impacts on seasonal precipitation, extreme events, and possible effects of climate change. *Stoch. Environ. Res. Risk Assessment* **25**, 537–554 (2011).
61. Cai, W. et al. Climate impacts of the El Niño–Southern Oscillation on South America. *Nat. Rev. Earth Environ.* **1**, 215–231 (2020).
62. Reboita, M. S., da Rocha, R. P., Ambrizzi, T. & Gouveia, C. D. Trend and teleconnection patterns in the climatology of extratropical cyclones over the Southern Hemisphere. *Clim. Dyn.* **45**, 1929–1944 (2015).
63. Collazo, S., Barrucand, M. & Rusticucci, M. Hot and dry compound events in South America: present climate and future projections, and their association with the Pacific Ocean. *Natl. Hazards* **119**, 299–323 (2023).
64. Silva, G. A. M., Ambrizzi, T. & Marengo, J. A. Observational evidences on the modulation of the South American Low Level Jet east of the Andes according the ENSO variability. *Ann Geophys* **27**, 645–657 (2009).
65. Montini, T. L., Jones, C. & Carvalho, L. M. V. The South American low-level jet: A new climatology, variability, and changes. *J. Geophys. Res.: Atmos.* **124**, 1200–1218 (2019).
66. Vasconcellos, F. C. et al. Warming trends of southwestern Atlantic SST and the summer's warmest SST's impact on South American climate. *Int. J. Climatol.* **43**, 5604–5619 (2023).
67. Mantua, N. J. & Hare, S. R. The Pacific decadal oscillation. *J. Oceanogr.* **58**, 35–44 (2002).
68. Jiang, S., Zhu, C., Hu, Z.-Z., Jiang, N. & Zheng, F. Triple-dip La Niña in 2020–23: understanding the role of the annual cycle in tropical Pacific SST. *Environ. Res. Lett.* **18**, 084002 (2023).
69. Kayano, M. T. & Andreoli, R. V. Relations of South American summer rainfall interannual variations with the Pacific Decadal Oscillation. *Int. J. Climatol.* **27**, 531–540 (2007).
70. Wang, S., Huang, J., He, Y. & Guan, Y. Combined effects of the Pacific Decadal Oscillation and El Niño-Southern Oscillation on Global Land Dry–Wet Changes. *Sci. Rep*. **4**, 6651 (2014).
71. Grotjahn, R. General Circulation of the Atmosphere | Energy Cycle. in *Encyclopedia of Atmospheric Sciences* 51–64. https://doi.org/10.1016/B978-0-12-382225-3.00155-9 (Elsevier, 2015).
72. Schielicke, L. & Pfahl, S. European heatwaves in present and future climate simulations: a Lagrangian analysis. *Weather Clim. Dyn.* **3**, 1439–1459 (2022).

73. Röthlisberger, M. & Papritz, L. Quantifying the physical processes leading to atmospheric hot extremes at a global scale. *Nat. Geosci.* **16**, 210–216 (2023).
74. Yiou, P., Vautard, R., Naveau, P. & Cassou, C. Inconsistency between atmospheric dynamics and temperatures during the exceptional 2006/2007 fall/winter and recent warming in Europe. *Geophys. Res. Lett.* **34**, L21808 (2007).
75. Cattiaux, J. et al. Winter 2010 in Europe: A cold extreme in a warming climate. *Geophys. Res. Lett*. **37**, L20704 (2010).
76. Vautard, R. et al. Attribution of human-induced dynamical and thermodynamical contributions in extreme weather events. *Environ. Res. Lett.* **11**, 114009 (2016).
77. Yiou, P. et al. A statistical framework for conditional extreme event attribution. *Adv. Stat Climatol Meteorol Oceanogr.* **3**, 17–31 (2017).
78. Jézéquel, A., Yiou, P. & Radanovics, S. Role of circulation in European heatwaves using flow analogues. *Clim. Dyn.* **50**, 1145–1159 (2018).
79. IPCC AR6. Weather and Climate Extreme Events in a Changing Climate. in *Climate Change 2021 – The Physical Science Basis* 1513–1766. https://doi.org/10.1017/9781009157896.013 (Cambridge University Press, 2023).
80. Feron, S. et al. Observations and projections of heat waves in South America. *Sci. Rep.* **9**, 8173 (2019).
81. Rusticucci, M., Kyselý, J., Almeira, G. & Lhotka, O. Long-term variability of heat waves in Argentina and recurrence probability of the severe 2008 heat wave in Buenos Aires. *Theor. Appl. Climatol* **124**, 679–689 (2016).
82. Ceccherini, G., Russo, S., Ameztoy, I., Romero, C. P. & Carmona-Moreno, C. Magnitude and frequency of heat and cold waves in recent decades: the case of South America. *Natl. Hazards Earth Syst. Sci.* **16**, 821–831 (2016).
83. Hannart, A., Vera, C., Cerne, B. & Otto, F. E. L. Causal Influence of Anthropogenic Forcings on the Argentinian Heat Wave of December 2013. *Bull. Am. Meteorol. Soc.* **96**, S41–S45 (2015).
84. Otto, F. E. L., Skeie, R. B., Fuglestvedt, J. S., Berntsen, T. & Allen, M. R. Assigning historic responsibility for extreme weather events. *Nat. Clim. Change* **7**, 757–759 (2017).
85. Miranda, V. F. V. V. et al. Heat stress in South America over the last four decades: a bioclimatic analysis. *Theor. Appl. Climatol* https://doi.org/10.1007/s00704-023-04668-x (2023).
86. Miralles, D. G., Teuling, A. J., Van Heerwaarden, C. C. & De Arellano, J. V. G. Mega-heatwave temperatures due to combined soil desiccation and atmospheric heat accumulation. *Nat. Geosci.* **7**, 345–349 (2014).
87. Diro, G. T. et al. Land-atmosphere coupling over North America in CRCM5. *J. Geophys. Res. Atmos.* **119**, 11955–11972 (2014).
88. Penalba, O. C. & Rivera, J. A. Precipitation response to El Niño/La Niña events in Southern South America – emphasis in regional drought occurrences. *Adv. Geosci.* **42**, 1–14 (2016).
89. Geng, T. et al. Increased occurrences of consecutive La Niña events under global warming. *Nature* **619**, 774–781 (2023).
90. IPCC AR6. Changing State of the Climate System. in *Climate Change 2021 – The Physical Science Basis* 287–422. https://doi.org/10.1017/9781009157896.004 (Cambridge University Press, 2023).
91. Chesini, F. et al. Mortality risk during heat waves in the summer 2013-2014 in 18 provinces of Argentina: Ecological study. *Cien Saude Colet* **27**, 2071–2086 (2022).
92. Hartinger, S. M. et al. The 2022 South America report of The Lancet Countdown on health and climate change: trust the science. Now that we know, we must act. *The Lancet Regional Health - Americas* **20**, 100470 (2023).
93. Santágata, D. M., Castesana, P. & Rössler, C. E. & Gómez, D. R. Extreme temperature events affecting the electricity distribution system of the metropolitan area of Buenos Aires (1971–2013). *Energy Policy* **106**, 404–414 (2017).
94. Buenos Aires Herald. Scientists: high temperatures due to climate change worsen impact of Argentina's drought. https://buenosairesherald.com/business/agro/scientists-high-temperatures-due-to-climate-change-worsen-impact-of-argentinas-drought.
95. Hersbach, H. et al. The ERA5 global reanalysis. *Quart. J. R. Meteorol. Soc.* **146**, 1999–2049 (2020).
96. Jendritzky, G., de Dear, R. & Havenith, G. UTCI—Why another thermal index? *Int. J. Biometeorol* **56**, 421–428 (2012).
97. Bröde, P. et al. Deriving the operational procedure for the Universal Thermal Climate Index (UTCI). *Int. J. Biometeorol* **56**, 481–494 (2012).
98. Zare, S. et al. Comparing Universal Thermal Climate Index (UTCI) with selected thermal indices/environmental parameters during 12 months of the year. *Weather Clim. Extrem* **19**, 49–57 (2018).
99. Bitencourt, D. P., Fuentes, M. V., Franke, A. E., Silveira, R. B. & Alves, M. P. A. The climatology of cold and heat waves in Brazil from 1961 to 2016. *Int. J. Climatol.* **40**, 2464–2478 (2020).
100. Perkins, S. E. & Alexander, L. V. On the measurement of heat waves. *J. Clim.* **26**, 4500–4517 (2013).
101. Sánchez-Benítez, A., García-Herrera, R., Barriopedro, D., Sousa, P. M. & Trigo, R. M. June 2017: The Earliest European Summer Mega-heatwave of Reanalysis Period. *Geophys. Res. Lett*. **45**, 1955–1962 (2018).
102. Carroll, E. B. Use of dynamical concepts in weather forecasting. *Meteorol. Appl.* **4**, S1350482797000583 (1997).
103. Stein, A. F. et al. NOAA's HYSPLIT atmospheric transport and dispersion modeling system. *Bull. Am. Meteorol. Soc.* **96**, 2059–2077 (2015).
104. van Haren, R., van Oldenborgh, G. J., Lenderink, G. & Hazeleger, W. Evaluation of modeled changes in extreme precipitation in Europe and the Rhine basin. *Environ. Res. Lett.* **8**, 014053 (2013).
105. Salazar, A., Baldi, G., Hirota, M., Syktus, J. & McAlpine, C. Land use and land cover change impacts on the regional climate of non-Amazonian South America: A review. *Glob. Planet Change* **128**, 103–119 (2015).
106. Mao, K. B. et al. Global aerosol change in the last decade: An analysis based on MODIS data. *Atmos. Environ.* **94**, 680–686 (2014).
107. Wilks, D. S. *Statistical Methods in the Atmospheric Sciences*. (Academic Press, London, 2019).
108. Wickham, H. *Ggplot2: Elegant Graphics for Data Analysis*. (Springer-Verlag New York, 2016).

Acknowledgements

This work was funded by the European Union's Horizon 2020 research and innovation program under the Marie Skłodowska-Curie grant agreement No 847635 (UNA4CAREER) through the SAFETE project (code 4230420). This work is part of the activities of the CSIC's Interdisciplinary Thematic Platform Clima (PTI Clima). This research was also supported by predoctoral grant program from the Comunidad de Madrid (No. PIPF-2022/ECO-25310).

Author contributions

All the authors designed the study. S.C., S.S. and P.Z. wrote the initial manuscript draft. S.C., S.S. and P.Z. conducted the experiments and produced the figures. S.C., S.S., P.Z., R.G.H., D.B. and J.M.G.P. contributed to the interpretation of the results. J.M.G.P. provided scripts for the analysis of the data. S.C., S.S., P.Z., R.G.H., D.B. and J.M.G.P. organized, revised, and edited the manuscript until its final version.

Competing interests

The authors declare no competing interests.

Additional information

Supplementary information The online version contains supplementary material available at https://doi.org/10.1038/s43247-024-01386-8.

Correspondence and requests for materials should be addressed to Soledad Collazo.

Peer review information *Communications Earth & Environment* thanks Chi-Cherng Hong and the other, anonymous, reviewer(s) for their contribution to the peer review of this work. Primary Handling Editors: Min Hui Lo, Heike Langenberg. A peer review file is available.